Coupled Simulation of Transport Phenomena in Directionally Solidifying γ(TiAl) Alloy under Electromagnetic Fields

The Transport Phenomena here are described in term of Temperature, Melt Flow Velocity, Pressure, Solid-Volume Fraction and Concentration Fields *etc*

Daming Xu[1], *Yunfeng Bai*[1], *Jingjie Guo*[1], *Liu Lin*[2] *and Hengzhi Fu*[1,2]

School of Materials and Engineering, [1)]Harbin Institute of Technology, [2)]Northwestern Polytechnological University

Contact E-mail: damingxu@hit.edu.cn

INTRODUCTION

- Heat energy and species mass transfer, as well as melt flow are basic transport phenomena in solidification processes of various alloy ingots and castings (called “ ***Solidification Transport Phenomena*** (**STP**)”).
- These phenomena, in turn, play a critical role in controlling the solidification behaviors, structures and various defects formations, such as macrosegregation and porosity *etc*.

- In order to improve the qualities of the solidified alloy ingots/materials or to develop new materials processing methods, various electromagnetic (**EM**) techniques have been applied to materials solidification processes.
- Such as: Using ***alternating EM inductors*** or ***EM stirrers/brakes in continuous casting*** of Al alloy/steel ingots for melt flow/meniscus shape controls, or using an ***EM-inducted cold-crucible technique*** to obtain directionally solidified γ(TiAl)-base alloy ingots/materials (currently studied in the authors' research group).

- In such ***EM materials processing*** applications, the EM-induced solidification heat/mass transfer, and especially the melt flow behaviors can be ***highly enhanced*** (or ***suppressed*** in the case of a static magnetic field applied), through the ***Lorentz forces*** and ***Joule heats***, and might be in a much more complex pattern.

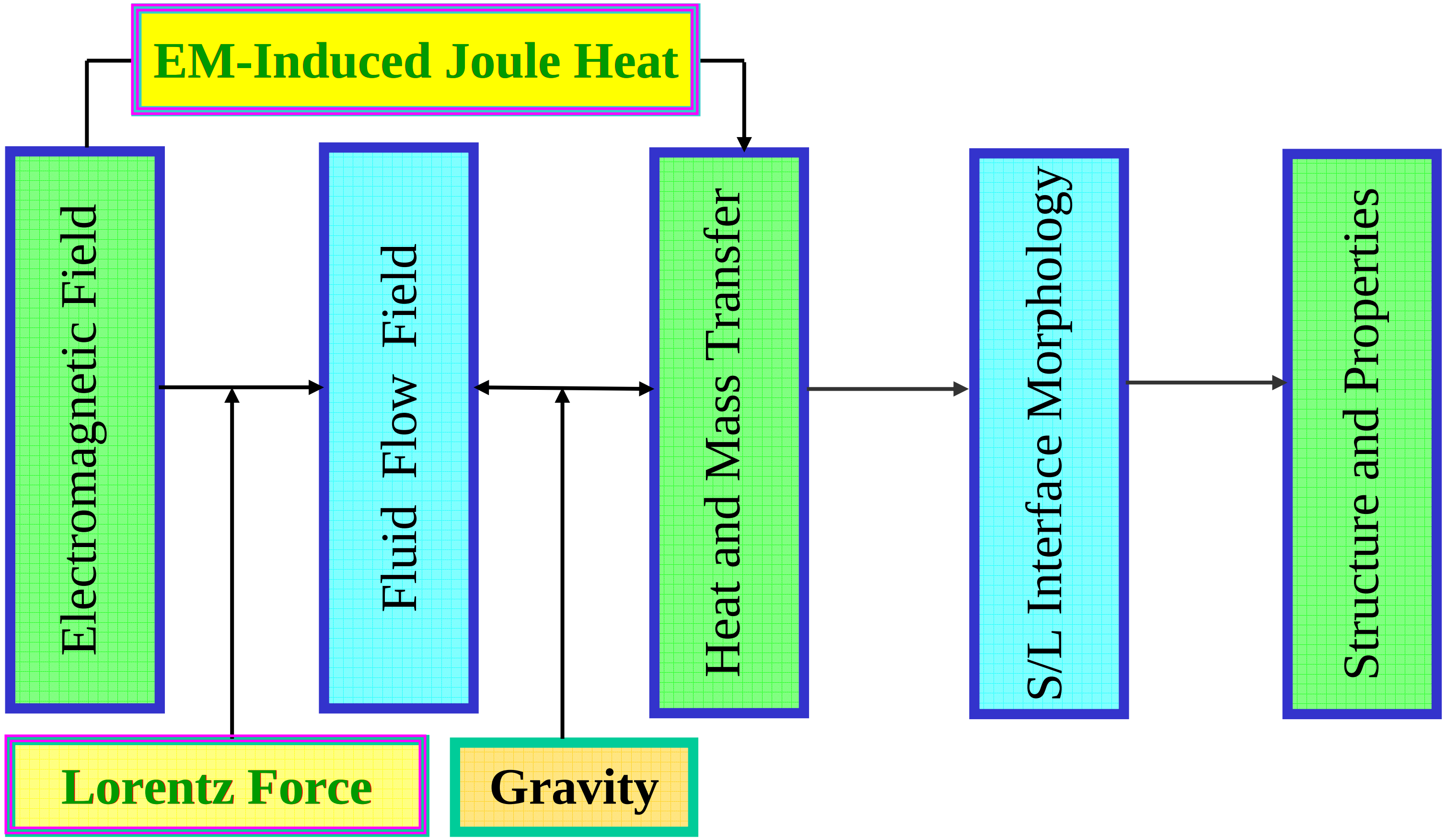

The Aim of This Presentation

To present: An efficient multifield-coupled modeling method for the STP in alloy ingots/materials under an arbitrary EM-field, jointly using two different Computer Codes (One is FEM-Based/Commercial, another is FDM-based/Authors').

The Main Tasks:

1) To further extend a previous continuum solidification-model and the corresponding numerical solution algorithms(including an extended Direct-SIMPLE scheme for directly solving the EM-/gravity-/solidification-shrinkage-driven and strongly pressure-linked flow problems) to a more general EM-STP-case;

2) To propose an efficient technique for FEM→FDM data-conversion;

3) Try to apply the modeling to EM-directional solidification of Ti alloy castings/ingots.

Physical Model for EM-Directional Solidification

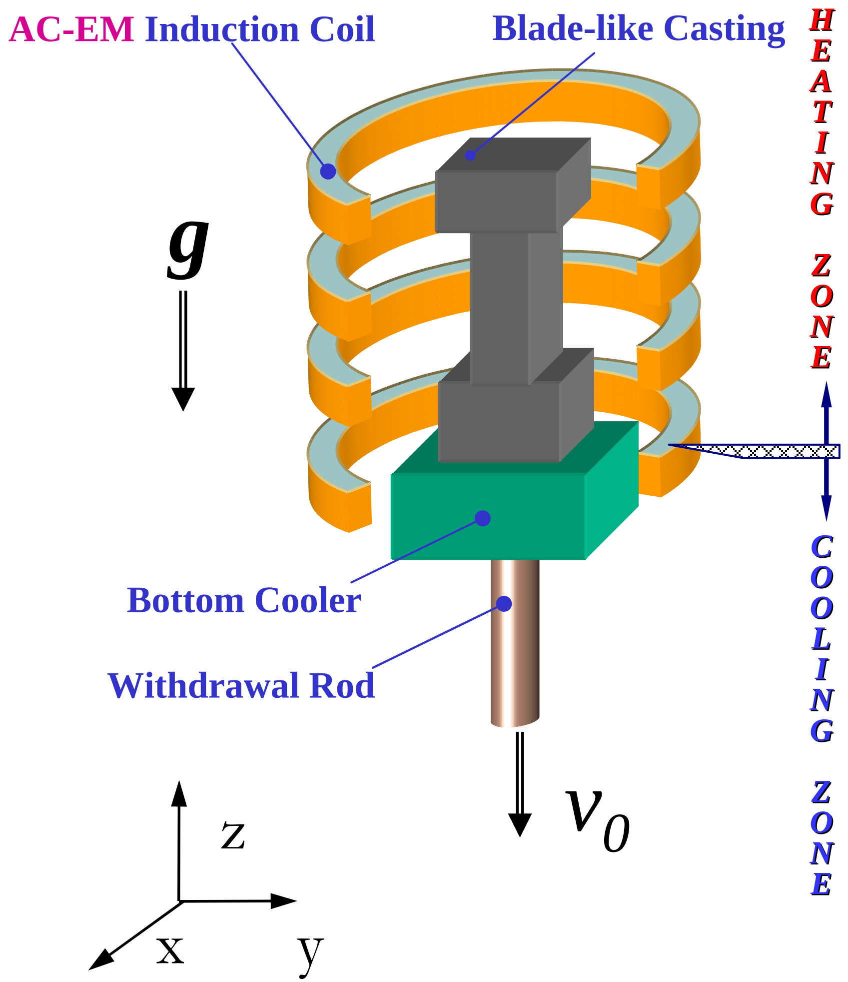

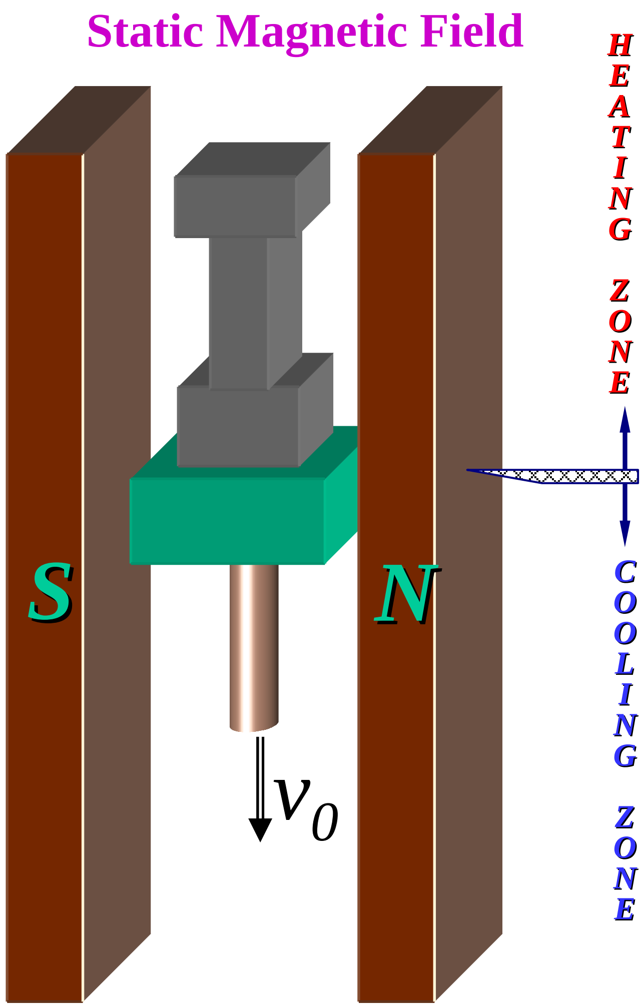

Electromagnetic solidification model

- **A Continuum Model** (based on Mixture Average Theory) with the following assumptions:

1) **the external forces involved in a solidifying system are gravity and Lorentz force;**
2) **no pores will occur, i.e. the geometric continuity, $f_L+f_S=1$, holds for any region in the casting/ingot domain;**
3) **the solid phase is macroscopically static during solidification;**
4) **local thermodynamic equilibrium holds at the microscopic solid-liquid interfaces**
5) **Newtonian and laminar liquid flow present;**
6) **the model alloy is a binary system.**

- ***Solidification heat energy transfer***

$$\partial[(\rho c_P)_m T]/\partial t + \nabla(f_L \rho_L c_{PL} V\ T) = \nabla[\lambda_m \nabla T] + \rho_S h(\partial f_S/\partial t) + q_J \quad (1)$$

where, the electromagnetically inducted Joule heat is given by

$$q_J = \mathbf{J}_G \mathbf{E} = \mathbf{J}_G^2/\sigma \quad (2)$$

- ***Solidification solute mass transfer***

$$\partial(\rho C)_m/\partial t + \nabla(f_L \rho_L V C_L) = \nabla[D_L \nabla(f_L \rho_L C_L) + D_S \nabla(f_S \rho_S C_S)] \quad (3)$$

where:

$$\partial(\rho C)_m/\partial t = (\rho_S C_S)^* \partial f_S/\partial t + \Phi f_S \partial(\rho_S C_S)^*/\partial t + (\rho_L C_L)\partial f_L/\partial t + f_L \partial(\rho_L C_L)/\partial t \quad (4)$$

$$\Phi = \theta\varphi/(1 + \theta\varphi), \quad \varphi = (D_S(T)/R_f)\zeta \cdot \mathbf{A}_{2N} \text{ and } \theta = k(1 + \beta)f_S/f_L^2$$

- ***L-S phase-change characteristic function for a specific alloy***

$$T_{Liq} = T_{Liq}(C_L^*) \quad (5)$$

- ***Solidification mass conservation:***

$$\partial\rho_m/\partial t = -\nabla(f_L\rho_L V) \quad (6)$$

where, $\partial\rho_m/\partial t \approx \rho_S^*\partial f_S/\partial t + \Phi f_S\partial\rho_S^*/\partial t + \rho_L\partial f_L/\partial t + f_L\partial\rho_L/\partial t$ (7)

- ***Momentum transfer for bulk/interdendritic liquid flow:***

$$\partial(f_L\rho_L V)/\partial t + \nabla[(f_L\rho_L V)\cdot V] = \nabla[\mu\nabla(f_L V)] - \nabla(f_L P) - (\mu f_L^2/K)V + F_B \quad (8)$$

For the present modeling, the body force term induced by external fields includes the gravity and Lorentz force:

$$\mathbf{F}_B = f_L\rho_L\mathbf{g} + \mathbf{F}_L \quad (9)$$

the Lorentz force acting on the moving liquid phase during solidification:

$$\mathbf{F}_L = \sigma f_L(\mathbf{E} + \mathbf{V}\times\mathbf{B})\times\mathbf{B} = f_L\{\mathbf{J}_G\times\mathbf{B} + \sigma[(\mathbf{V}\cdot\mathbf{B})\mathbf{B} - \mathbf{B}^2\mathbf{V}]\} \quad (10)$$

- ***Maxwell's equations***

$\nabla \times \mathbf{H} = \mathbf{J} + \partial \mathbf{D}/\partial t$ (*Law of Maxwell-Ampere*) (11)

$\nabla \times \mathbf{E} = -\partial \mathbf{B}/\partial t$ (*EM-Induction Law of Faraday*) (12)

$\nabla \cdot \mathbf{D} = \rho_e$ (*Law of Gauss*) (13)

$\nabla \cdot \mathbf{B} = 0$ (*Continuity of Magnetic Flux*) (14)

- ***Constitutive equations for the involved EM-medium materials***

$\mathbf{D} = \varepsilon \mathbf{E}$ (*Constitutive Relationship of Electric Properties*) (15)

$B = \mu H$ (*Constitutive Relationship of Magnetic Properties*) (16)

$\mathbf{J} = \sigma(\mathbf{E} + f_L \mathbf{V} \times \mathbf{B})$ (*Ohm Law for the Moving Metallic Melt*) (17)

Model Numerical Solution Strategy

- **Electromagnetic Fields** (***B*** and ***J*** vector fields *etc*)

  —— Solved by ***ANSYS 6.1*** in a ***FEM***-*Scheme*;

- **Solidification Transport Phenomena Equations** (scalar T, f_S, C_L, P and vector ***V*** fields)

  —— Solved by a ***FDM***-*Scheme-based* Computer Simulation Code (*developed by the present authors*)

Numerical Solution Methods to the Equations for Alloy Solidification Transport Processes

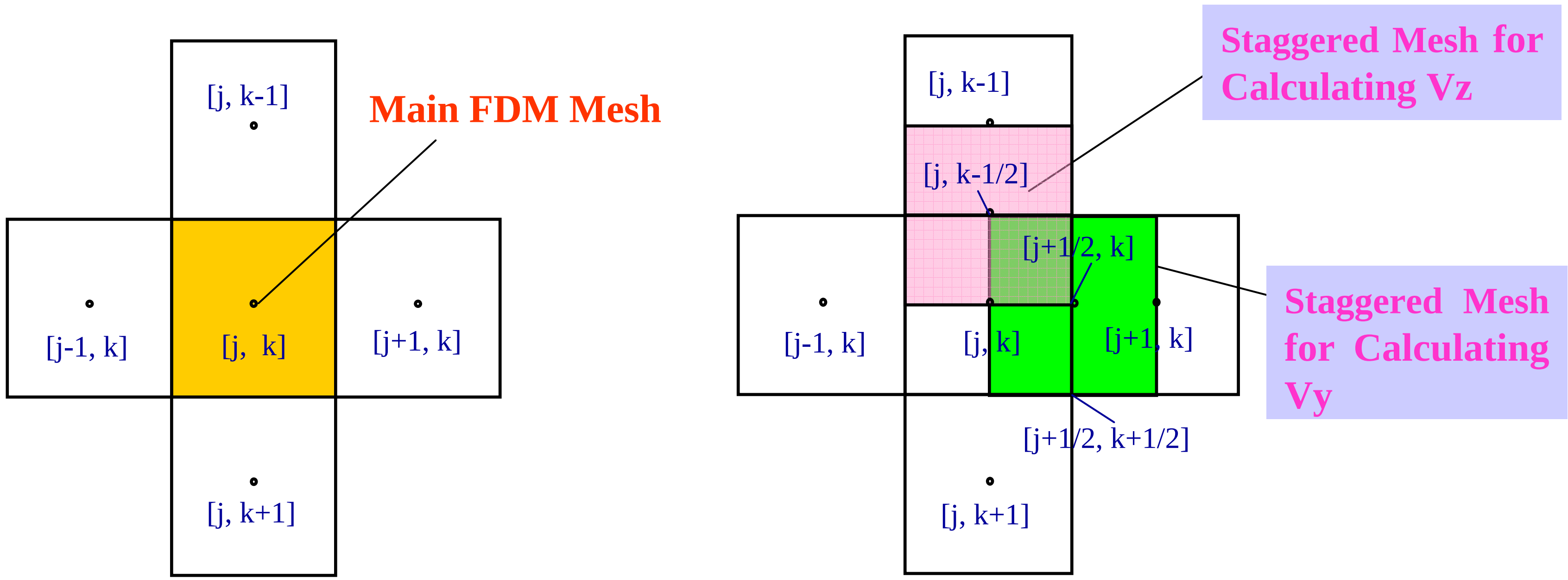

Main FDM Mesh [j,k] for Computations of the Scalar Variables T、f_S、C_L&P

Staggered Meshes [j+1/2, k] and [j, k-1/2] for Computations of the Vectorial Variables V_y&V_Z

Numerical Solution Methods to the Equations for Alloy Solidification Transport Processes

- Iterative Computations for the Nonlinear and Strong $T\text{–}f_S\text{–}C_L$ Coupling

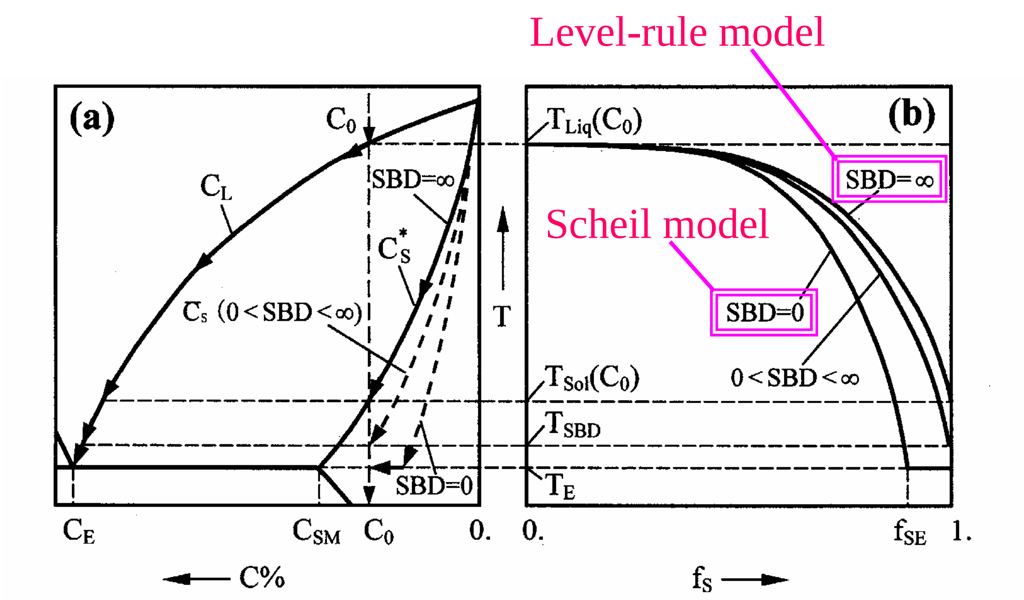

Figure 1 Solidification behaviors of a binary alloy of nominal composition $C_0<C_{SM}$ and with different solid-back diffusion (SBD) extents (Thermodynamic equilibrium holds at the micro-scale S/L interface). (a) A portion of binary alloy phase diagram with the solidification paths of C_L, C_S^* and $\bar{C}_S$ for different SBD; (b) The corresponding curves of solid fraction versus liquidus.

Available for ANY Solid Back-Diffusion

Available for BOTH Single-Phase and Eutectic Solidification Portions

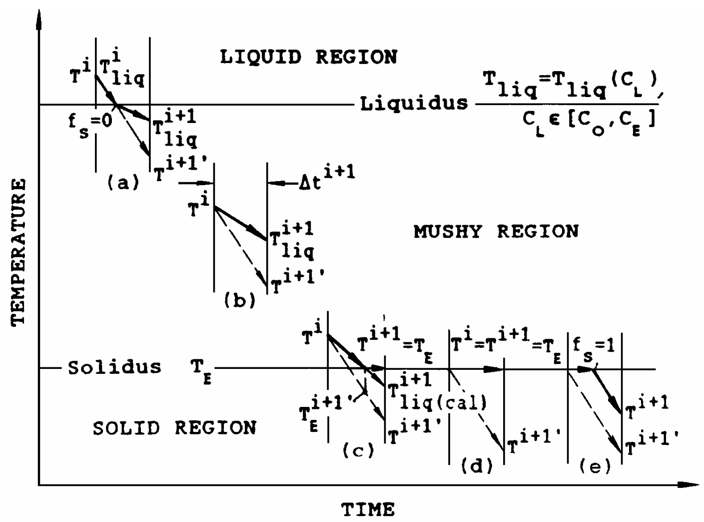

Fig. 4 Revised temperature by the latent heat release T^{i+1} (solid line) and the estimated temperature by Eq. (8) $T^{i+1'}$ (dashed line) for a control volume at the different nonequilibrium solidification stages for a binary eutectic system: *(a)* $f_S^i = 0$, $T^{i+1'} \le T_{liq}(C_0)$; *(b)* $f_{SE} > f_S^i > 0$, $T_{liq}(C_0) > T^{i+1'} \ge T_E$; *(c)* $0 < f_S^i < f_{SE}$ $(T^i > T_E)$, $T^{i+1'} < T_E$; *(d)* $1 > f_S^i \ge f_{SE}$ $(T^i = T_E)$, $T^{i+1'} < T_E$, $f_S^{i+1} < 1$; and *(e)* $1 > f_S^i > f_{SE}$, $T^{i+1'} < T_E$, $f_S^{i+1} = 1$.

(From: Daming Xu and Qingchun Li, " Numerical Method for Solution of Strongly Coupled Binary Aalloy Solidification Problems", *Numerical Heat Transfer, Part A*, 1991, Vol.20, 181-201.)

Numerical Solution Methods to the Equations for Alloy Solidification Transport Processes

- Calculations of the Nonlinear and Strong Pressure–Velocity (P–*V*) Coupling in a Solidification Transport Process of Alloy Casting/Ingot Takes Most Portion (>90%) of the Entire Computational Efforts for the STP Numerical Simulation;
- Therefore, it is of Great Importance to Adopt a Algorithm of High Computational Efficiency for a Practical STP-Based Computer Simulation for the Solidification Processes of Alloy Castings/Ingots.

Numerical Solution Methods to the Equations for Alloy Solidification Transport Processes

• Numerical Computations of the Nonlinear and Strong P–*V* Coupling

SIMPLE Scheme widely used for Fluid Transport Systems by *Subas V. Patankar*

Let $P = P^* + P'$, take an initial estimation: $P^o = P^*$

↓

Calculate the approximate velocity: V_X^* & V_Y^* based on the up-to-date pressure P^n and Momentum Equations

↓

Using V_X^*& V_Y^*, V-correction eqs. and mass-conserv. eq. to calculate the approximate pressure: P' and $P^{n+1} = P^n + P'$

↓

Using V_X^* , V_Y^*, P'&V-corr. eqs. to calculate approxi. V: V_X^{n+1}&V_Y^{n+1}; calculate other fields that influence P&*V*

↓

If P^{n+1}, V_X^{n+1} and V_Y^{n+1} converge?

No → $P^n = P^{n+1}$ (return to the velocity calculation)

Yes ↓

End of P-*V* coupling calculation

(From: Subas V. Patankar, *Numerical Heat Transfer and Fluid Flow*, McGraw-Hill, 1980)

Direct-SIMPLE Scheme by present Authors

(No Iteration Needed→C. Efficiency↑↑; Available both for P–*V* Coupling in Pure Fluid Systems and Alloy Solidification Systems)

Let: t^{i+1} time's pressure=t^i time's pressure + pressure change in the time interval Δt^{i+1}, i.e. $P^{i+1} = P^i + \Delta P^{i+1}$ (1)
Let: t^{i+1} time's accurate V-field=an approximate V-field + the V-corrections induced by the pressure change in time Δt^{i+1}: ΔP^{i+1},
i.e. $V_X^{i+1} = V_X^* + V_X'$ and $V_Y^{i+1} = V_Y^* + V_Y'$ (2)/(3)

↓

Using t^i time's pressure field: P^i and t^i time's V-field: V_x^i and V_Y^i, calculate the approxi. V-field: V_X^* and V_Y^* from momentum eqs.

↓

Using the obtained t^{i+1} time's T, f_S and C_L fields, and the approxi. V-field: V_X^*/V_Y^*, solve the algebraical eq. set for ΔP^{i+1} which is derived from the mass conservation eq. and the V-correction eqs.

↓

Using V_X^*、 V_Y^*&ΔP^{i+1} and the V-corr. eqs., calculate the accurate t^{i+1} time's pressure and velosity fieds: P^{i+1}&V^{i+1} from eqs.(1)-(3).

↓

End of P-*V* coupling calculation

(From: Daming Xu and Qingchun Li, " Gravity- and Solidification-Shrinkage-Induced Liquid Flow in a Horizontally Solidified Alloy Ingot", *Numerical Heat Transfer, Part A*, 1991, Vol.20, 203-221.)

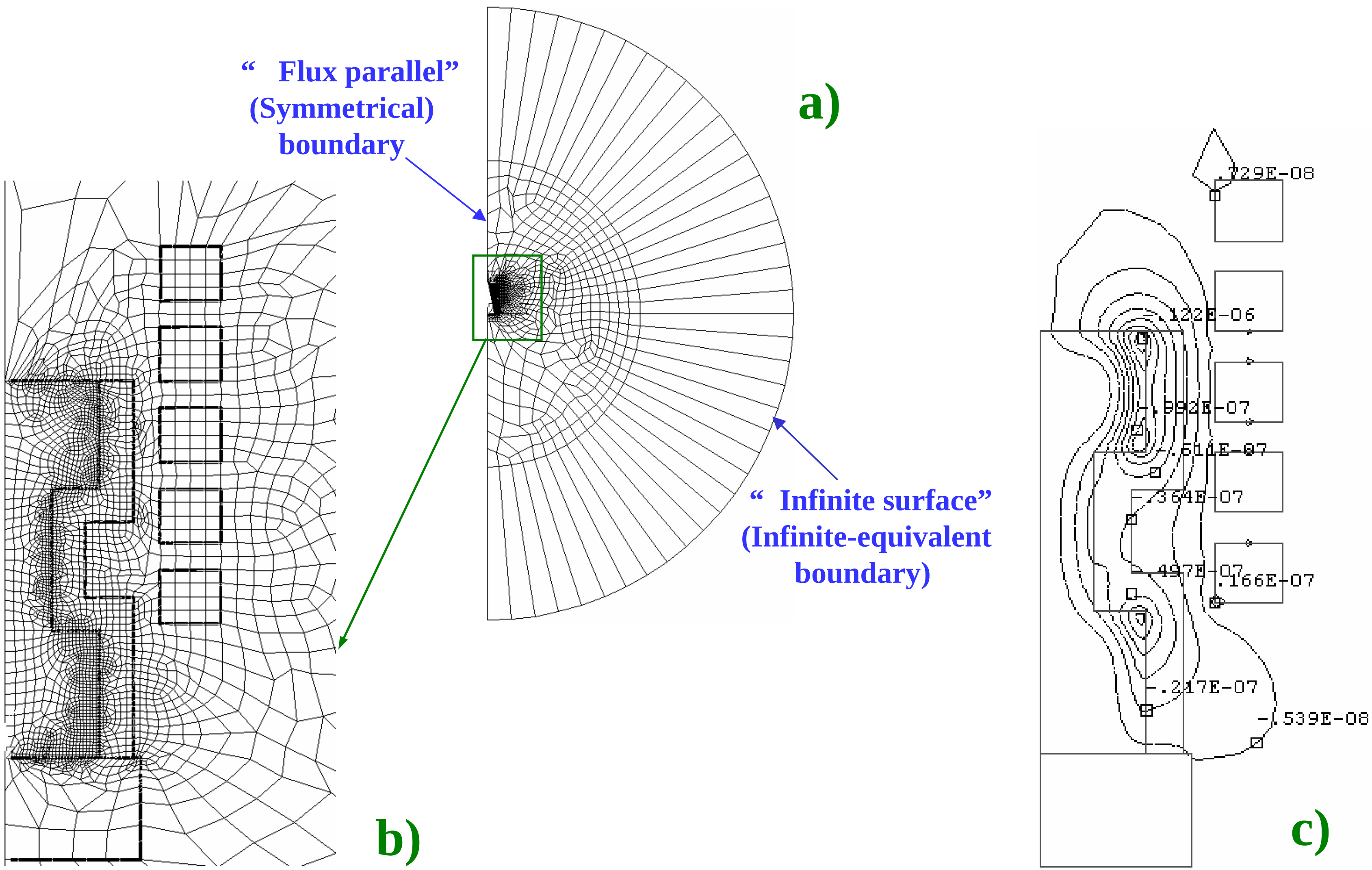

FEM-calculated results from **ANSYS 6.1** (TiAl casting, CaO mould, under a harmonic EM-field of 20kHz and with loads of 10kAt. The shaped casting has moved down for 40mm relative to the coils): **a)** meshed pattern for the whole EM-directional solidification system (right-half, with the EM-boundary definitions); **b)** the local meshed element grids around the casting; **c)** calculated distribution of the Az magnetic potential contours.

FEM-EM Results→FDM Format Conversion

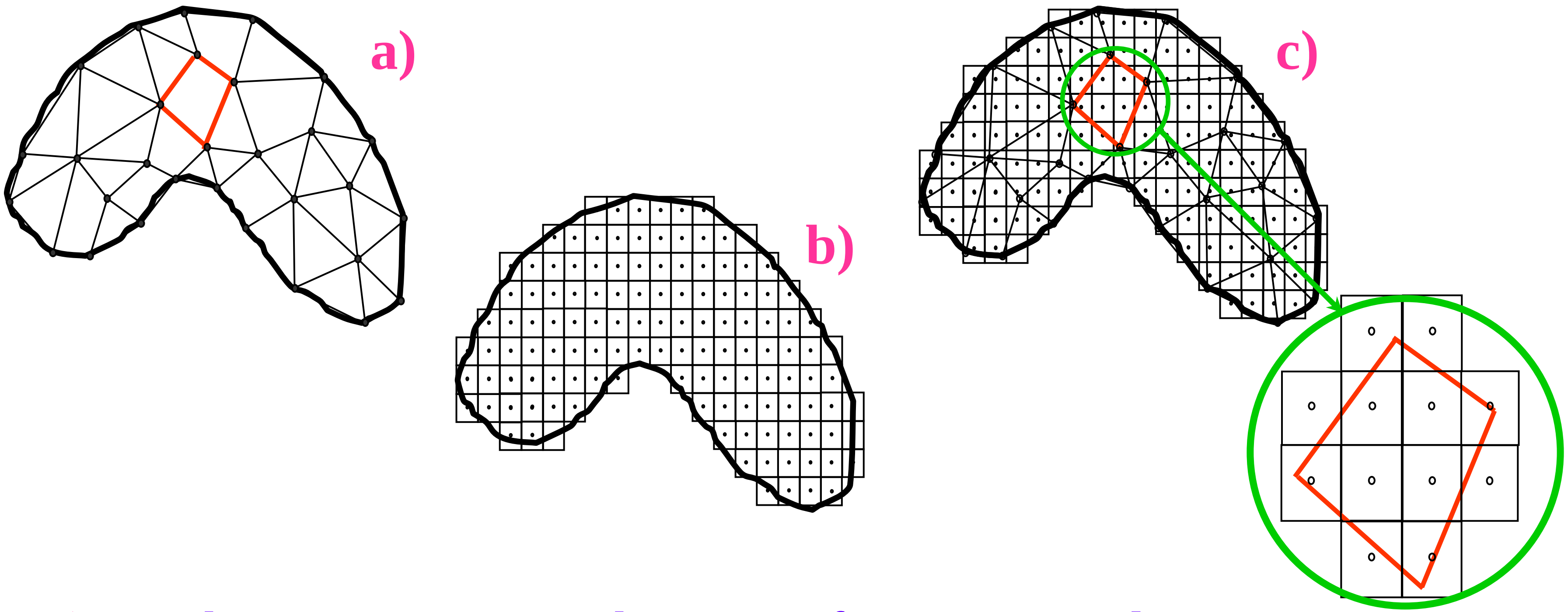

a) A schematic FEM mesh pattern for a casting domain;
b) A schematic FDM mesh pattern for the same casting domain;
c) Overlap of a) and b)

FEM-EM Results→FDM Format Conversion

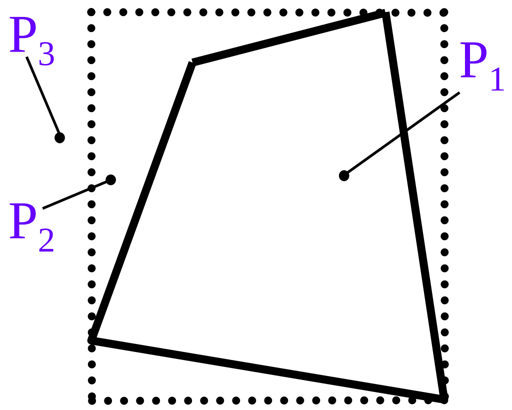

Maximum boundary of a FEM element (dot lines)

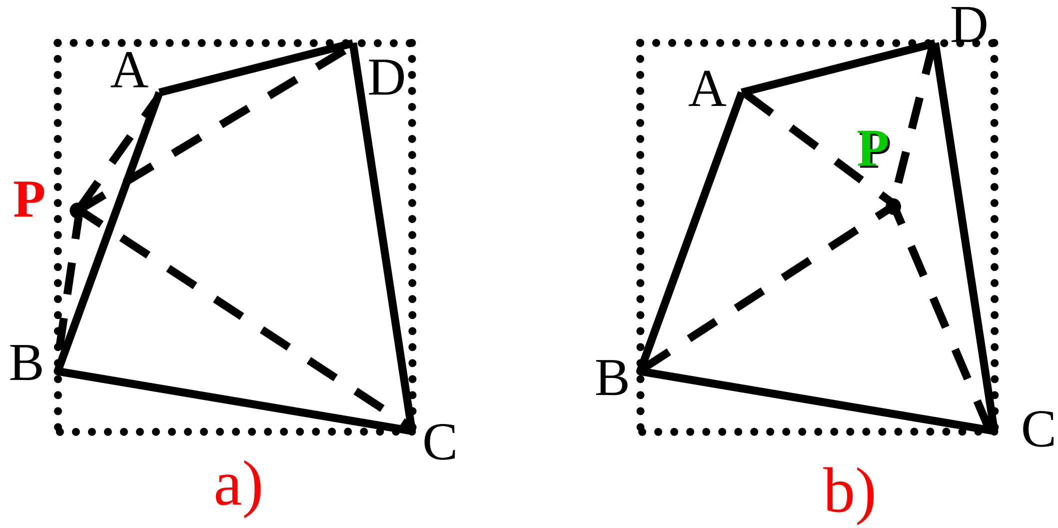

Method to judge if a FDM node P lies inside the FEM element ABCD.

Judgment:

IF [S (= S_{ADP} +S_{DCP} +S_{CBP} +S_{ABP}) = S_{ADCB}], THEN the FDM-node P is inside FEM-element ADCB; ELSE, the node P is outside the FEM-element.

FEM-EM Results→FDM Format Conversion

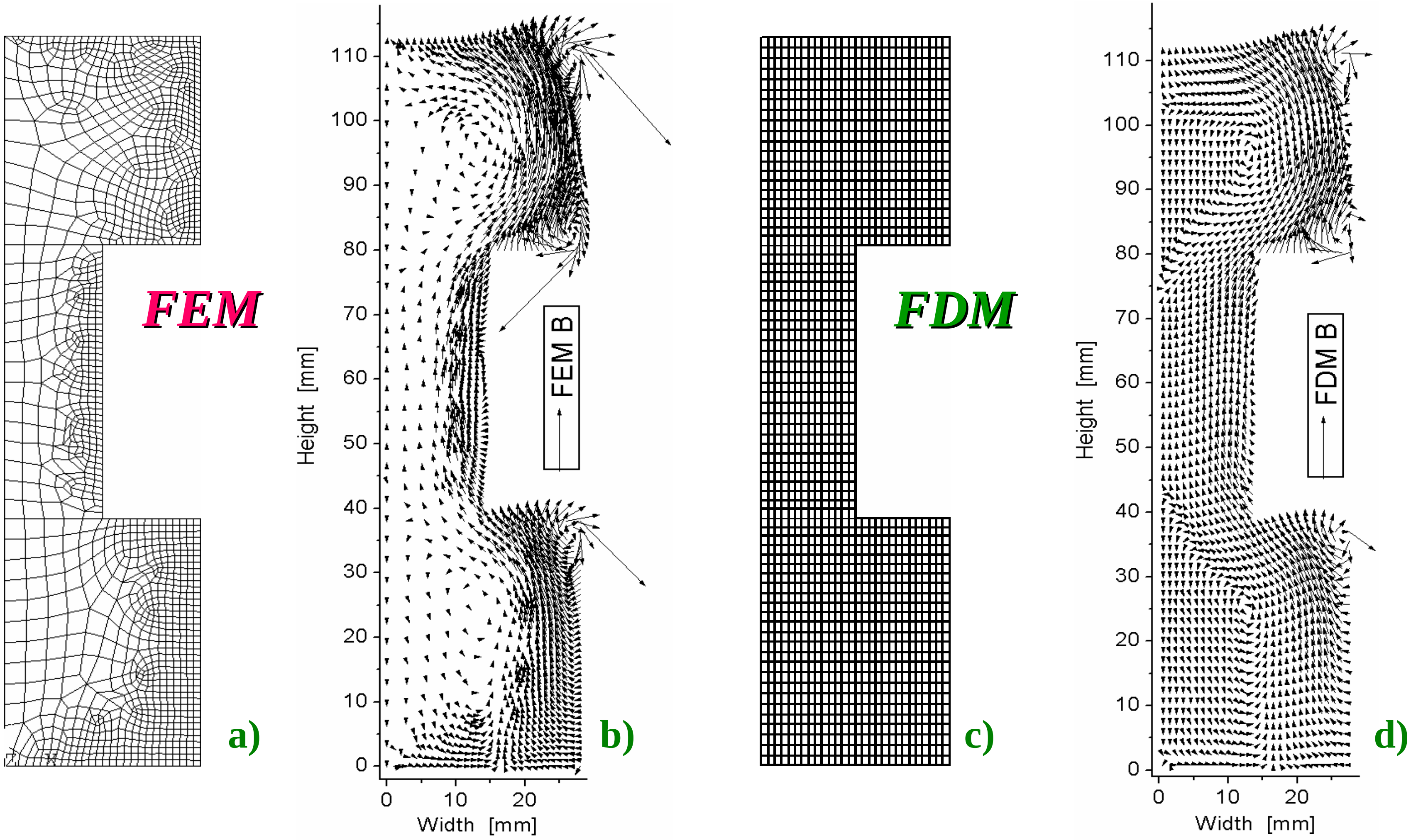

a) Meshed grids for ANSYS **FEM**-analysis, **b)** FEM magnetic flux density vectors, **c)** Meshed grids for the **FDM**-STP simulation, **d)** Converted magnetic flux density vectors

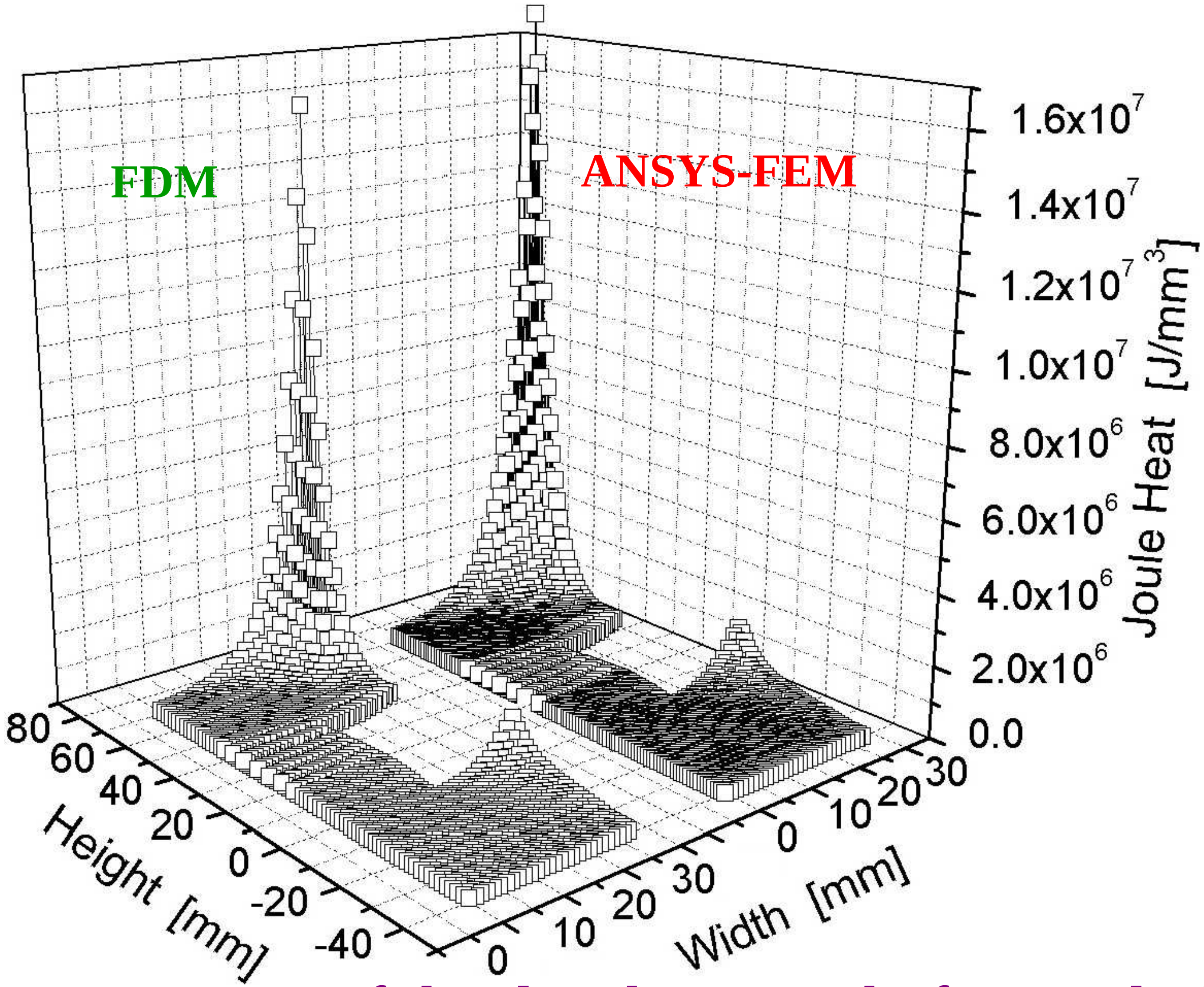

The comparison of the data between before and after conversion (**Joule Heat**)

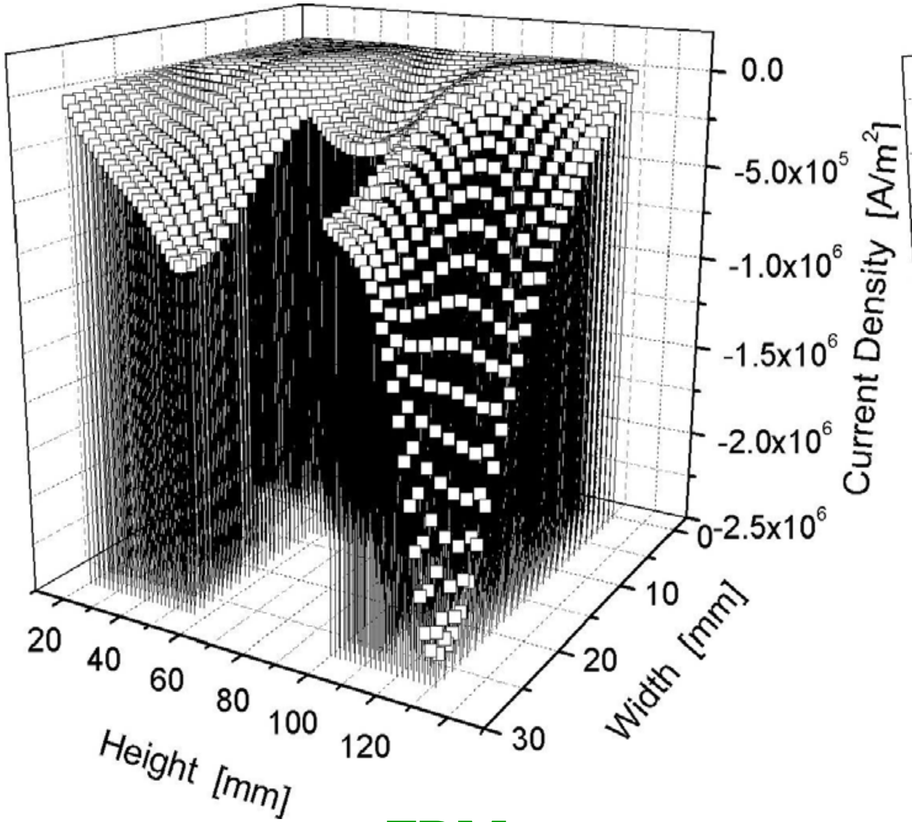

FDM

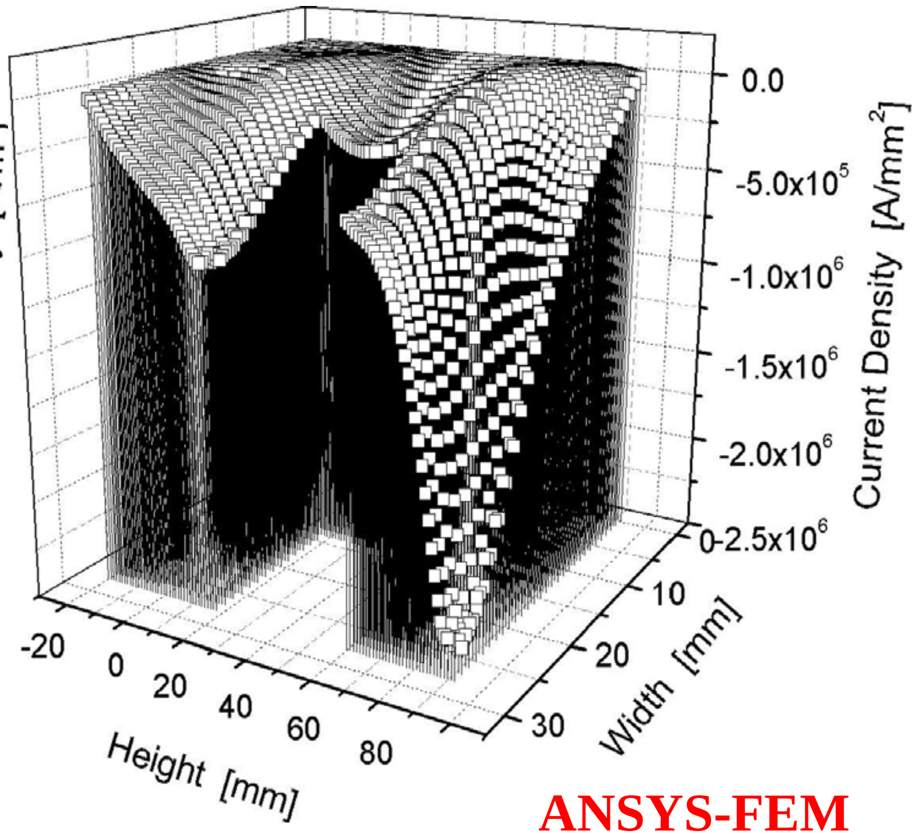

ANSYS-FEM

The comparison of the data between before and after conversion (**Inducted current density**)

The physical properties used for the present computer modeling of solidification transport phenomena of γ (TiAl)-Al%at. pseudo-binary alloy

- Thermal conductivity: $\lambda_S(T) = \lambda_L(T) = 2.3\times10^{-2}$ [W/mm·°C]
- Solid specific heat:

$$c_{PS}(T) = \begin{cases} 0.67832 - 6.4328\times10^{-6}\cdot T + 2.5417\times10^{-13}\cdot T^3, & (25°C < T \le 660°C) \\ 0.68286 + 1.3644\times10^{-5}\cdot T, & (660°C < T \le 882°C) \\ 0.65193 + 1.0513\times10^{-5}\cdot T, & (882°C < T \le 1490°C) \end{cases} \quad [J/g\cdot°C]$$

- Liquid specific heat: $c_{PL}(T,C_L) = 0.86074$, $(1490°C < T \le 2727°C)$ [J/g·°C]
- Solid density of the alloy: $\rho_S(T,C_L) = 3.8\times10^{-3}$, [g/mm³]
- Liquid density of the alloy:

$$\rho_L(T,C_L) = 3.632\times10^{-3} - 2.0\times10^{-7}\cdot(T - T_{liq.}) - 9.32\times10^{-6}\cdot(C_L - C_O) \quad [g/mm^3]$$

- Latent heat of fusion: $h(C_S) = 435.4$ [J/g]
- Liquidus of the γ(TiAl)-Al%at. alloys:

$$T_{liq}(C_{L/Al}) = 802.19745 + 23.01678\cdot C_L - 0.20279\cdot C_L^2, \quad (C_L \in [54.86, 74.61at.\%Al]) \quad [°C]$$

- Partition coefficient:

$$k(C_{L/Al}) = 69.24438-4.03153\cdot C_L+8.894\times10^{-2}\cdot C_L^2-8.70031\times10^{-4}\cdot C_L^3 + 3.18595\times10^{-6}\cdot C_L^4 \quad (C_L \in [54.86, 74.61at.\%Al]) \quad [-]$$

- Liquid diffusion coefficient: $D_{L/Al}(T°C) = 5\times10^{-3}$ [mm²/s]
- Solid diffusion coefficient: $D_{S/Al}(T°C) = 0.11\cdot\exp[-14504/(T+273.15)]$ [mm²/s]
- Dynamic viscosity coefficient: $\mu(T) = 3.5\times10^{-3}$ [Pa·s] (= [N·s/m²] = [g/mm·s])
- Permeability coefficient:

$$K = \begin{cases} 4.0\times10^{-4} f_L^{3.0}, & (f_L \le 0.7088) \\ 1.6318 f_L^{27.155}, & (0.7088 < f_L \le 0.99999) \\ 1.0\times10^{18}, & (f_L > 0.99999) \end{cases} \quad [mm^2]$$

- Primary dendrite spacing: $d_1 = 1.4\times10^{-1}$ [mm]
- Secondary dendrite arm spacing: $d_2 = 3.0\times10^{-2}$ [mm]

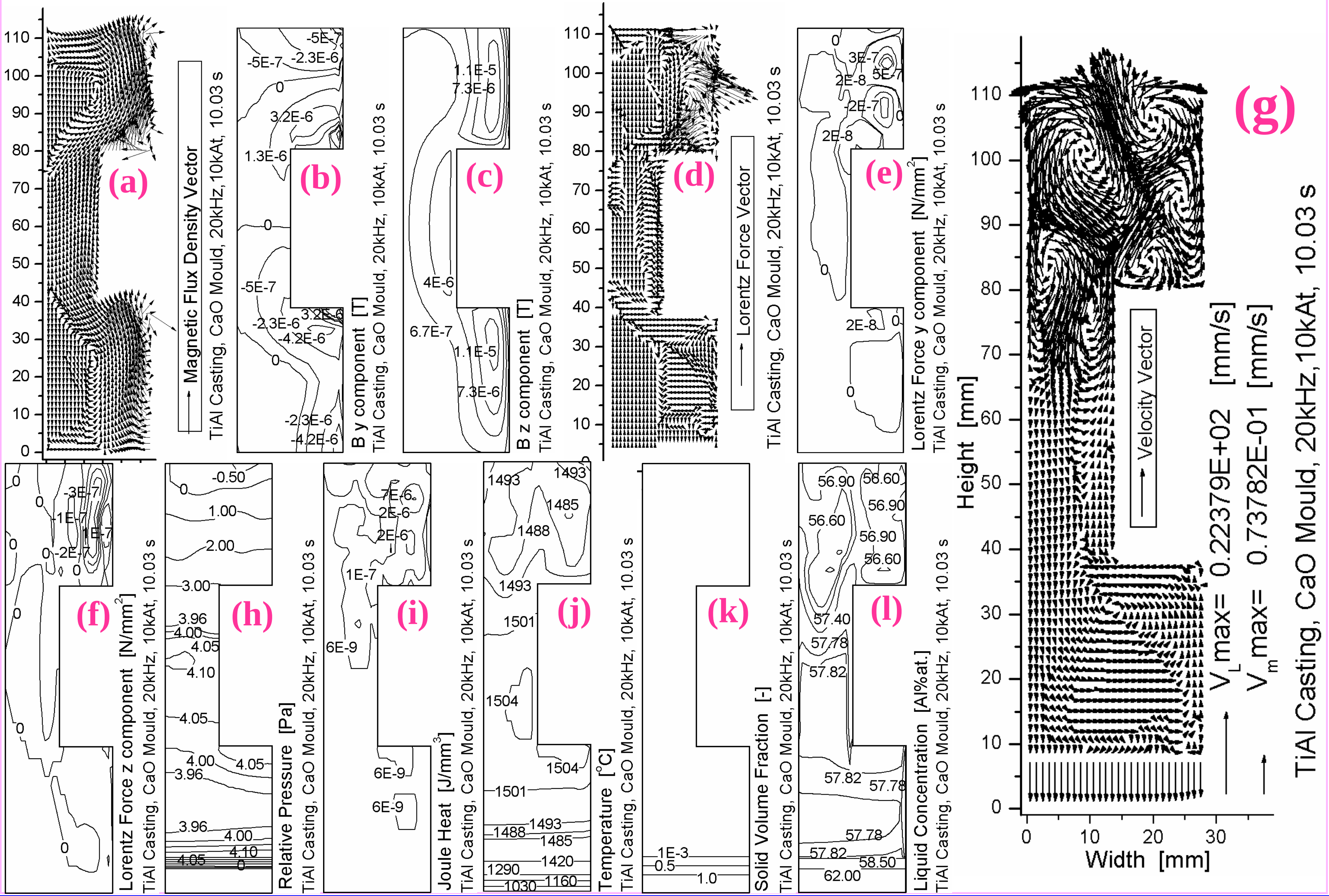

Directional STP of a γ(TiAl)-55at.%Al shaped casting under a harmonic EM-field: (a) FDM-converted/interpolated ***B*** vectors from ANSYS 6.1 FEM-results; (b) y-component of the ***B*** field; (c) z-component of the ***B*** field; (d) Lorentz force vectors; (e) y-component of the Lorentz force; (f) z-component of the Lorentz force; (g) velocity vectors of the alloy melt; (h) relative pressure contours of liquid phase; (i) contours of inducted Joule heat; (j) temperature contours; (k) contours of solid volume fraction; (l) liquid concentration contours for solute Al (at.%).

Directional Solidification Transport Behaviors under Harmonic EM-fields of Different Current Loads. γ(TiAl)-55Al%at. , 20kHz

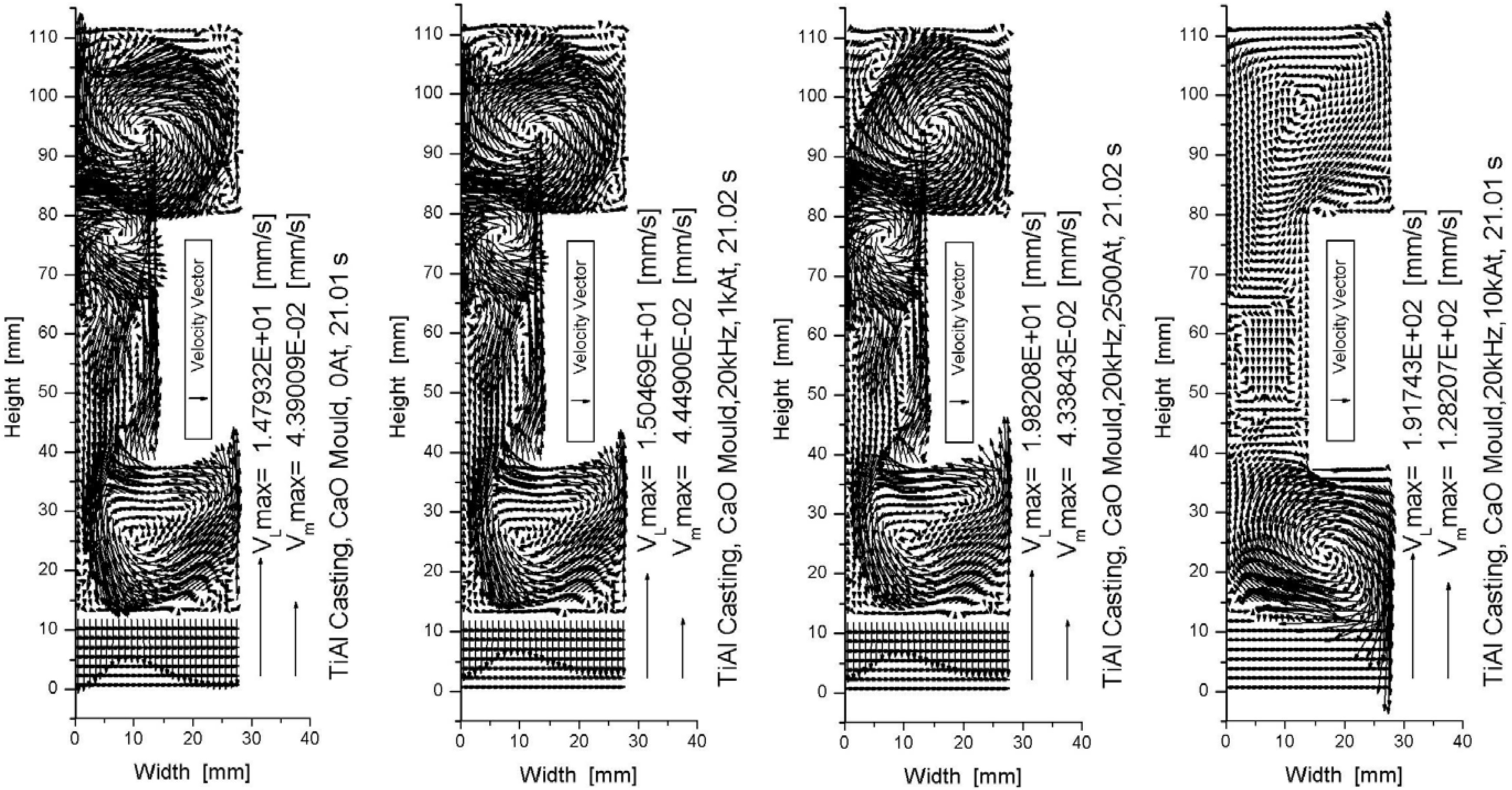

0At　　1000At　　2500At　　10000At

Melt Flow Velocity Vectors at ~21.0 sec

Directional Solidification Transport Behaviors under Harmonic EM-fields of Different Current Loads. γ(TiAl)-55Al%at. , 20kHz

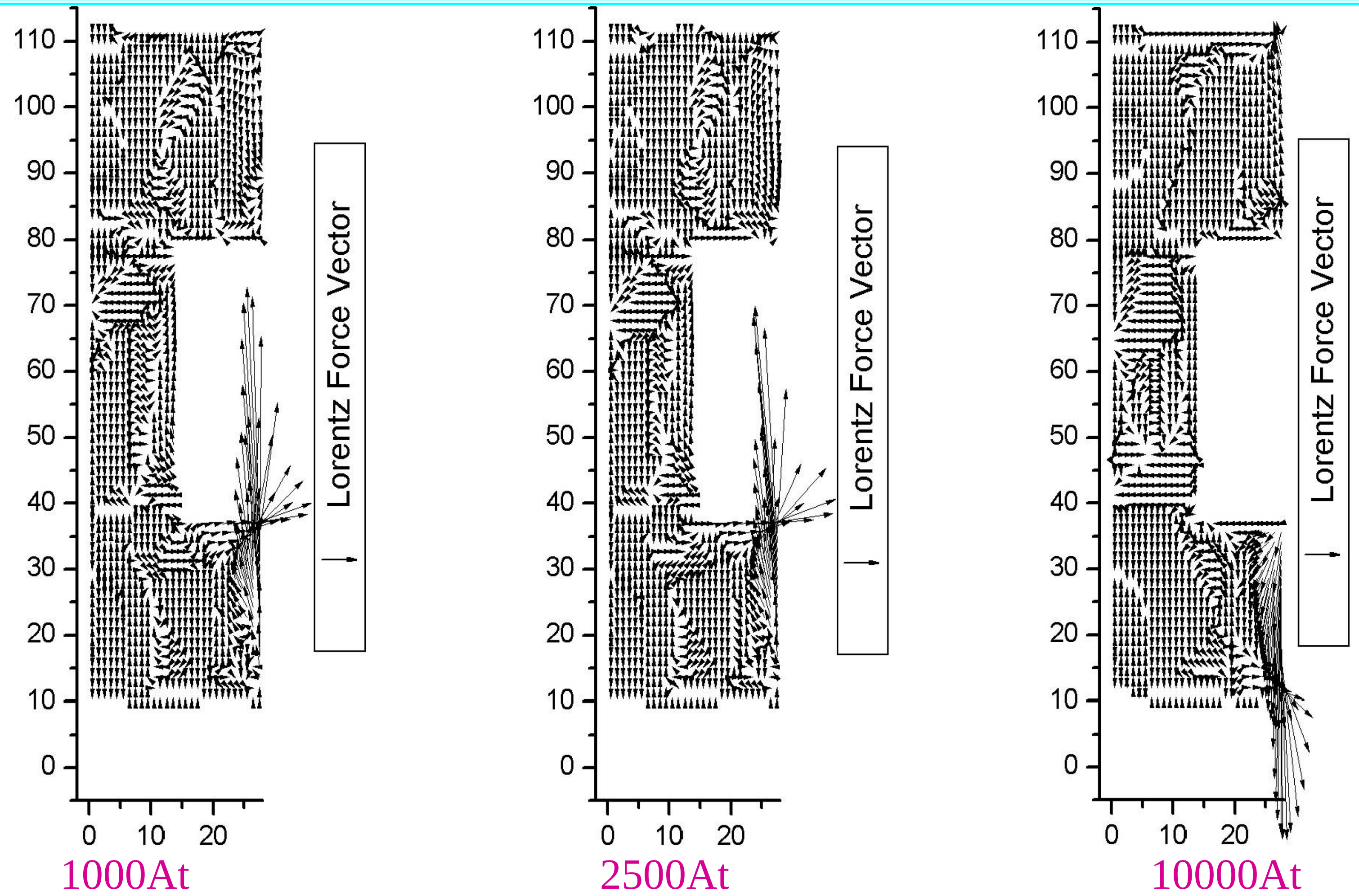

Lorentz Force Vectors at ~21.0 sec

Directional Solidification Transport Behaviors under Harmonic EM-fields of Different Current Loads. γ(TiAl)-55Al%at. , 20kHz

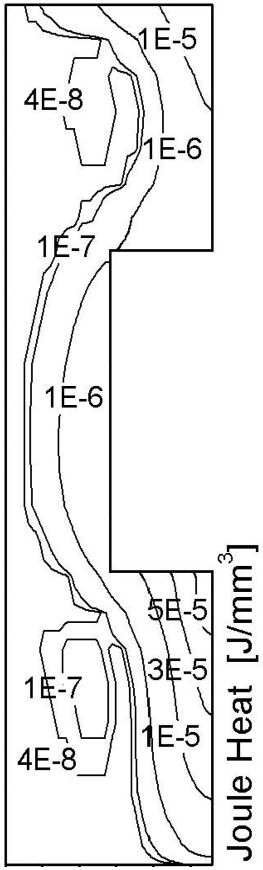

1000At

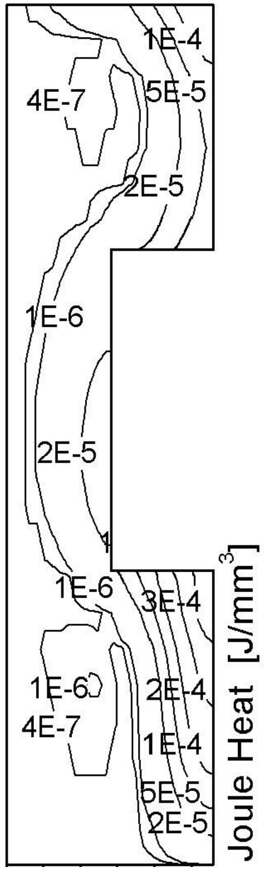

2500At

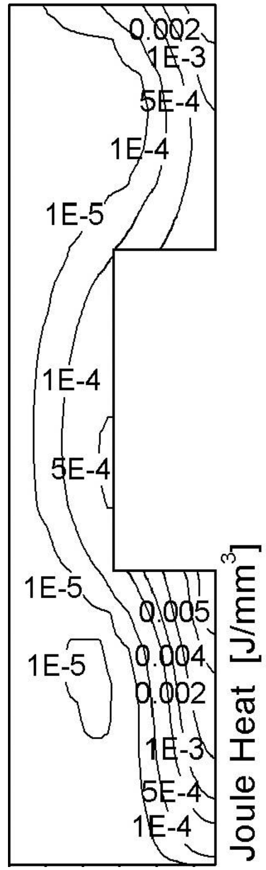

10000At

Contours of Joule Heat at ~21.0 sec

Directional Solidification Transport Behaviors under Harmonic EM-fields of Different Current Loads. γ(TiAl)-55Al%at. , 20kHz

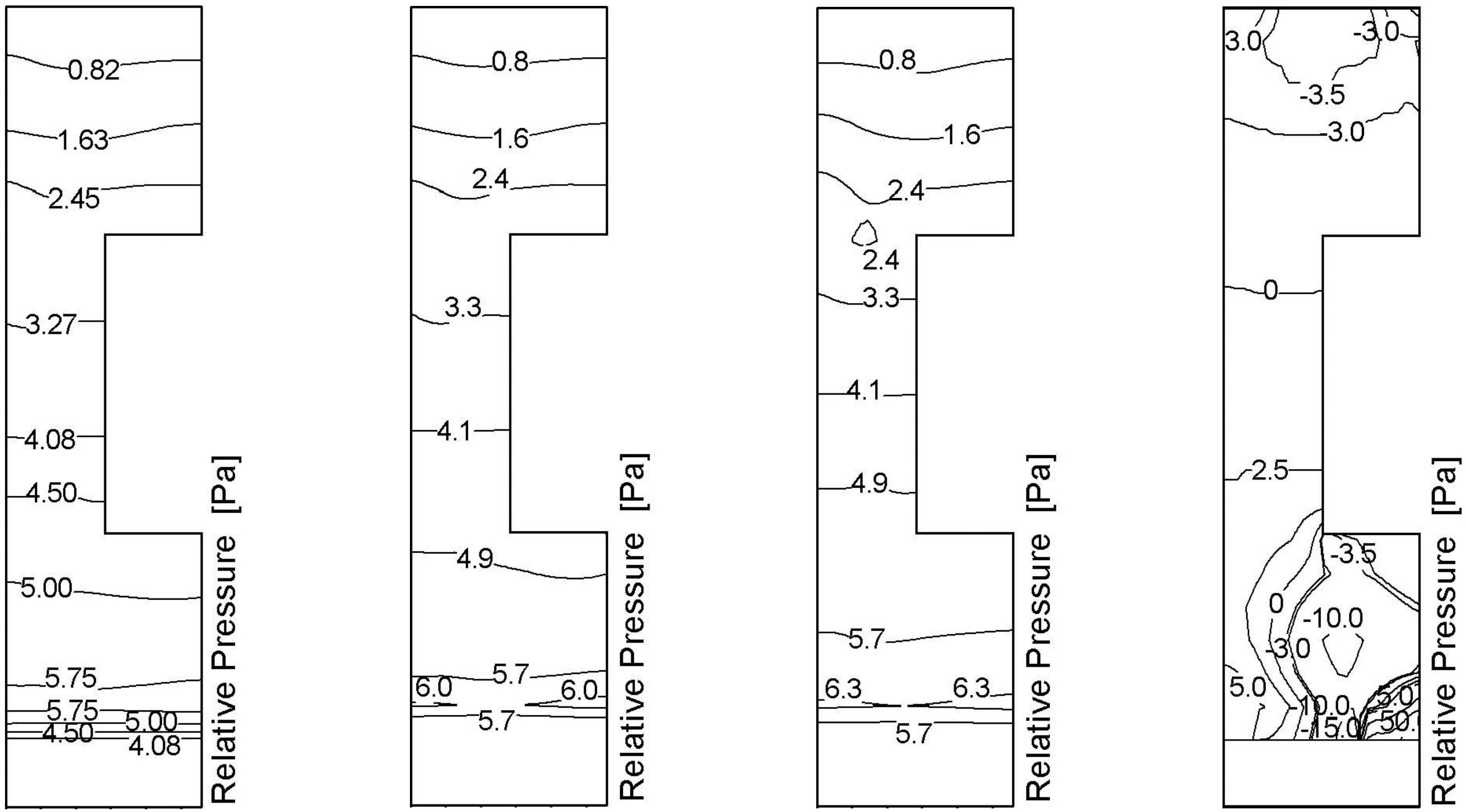

0At 1000At 2500At 10000At

Contours of Relative Pressure at ~21.0 sec

Directional Solidification Transport Behaviors under Harmonic EM-fields of Different Current Loads. γ(TiAl)-55Al%at. , 20kHz

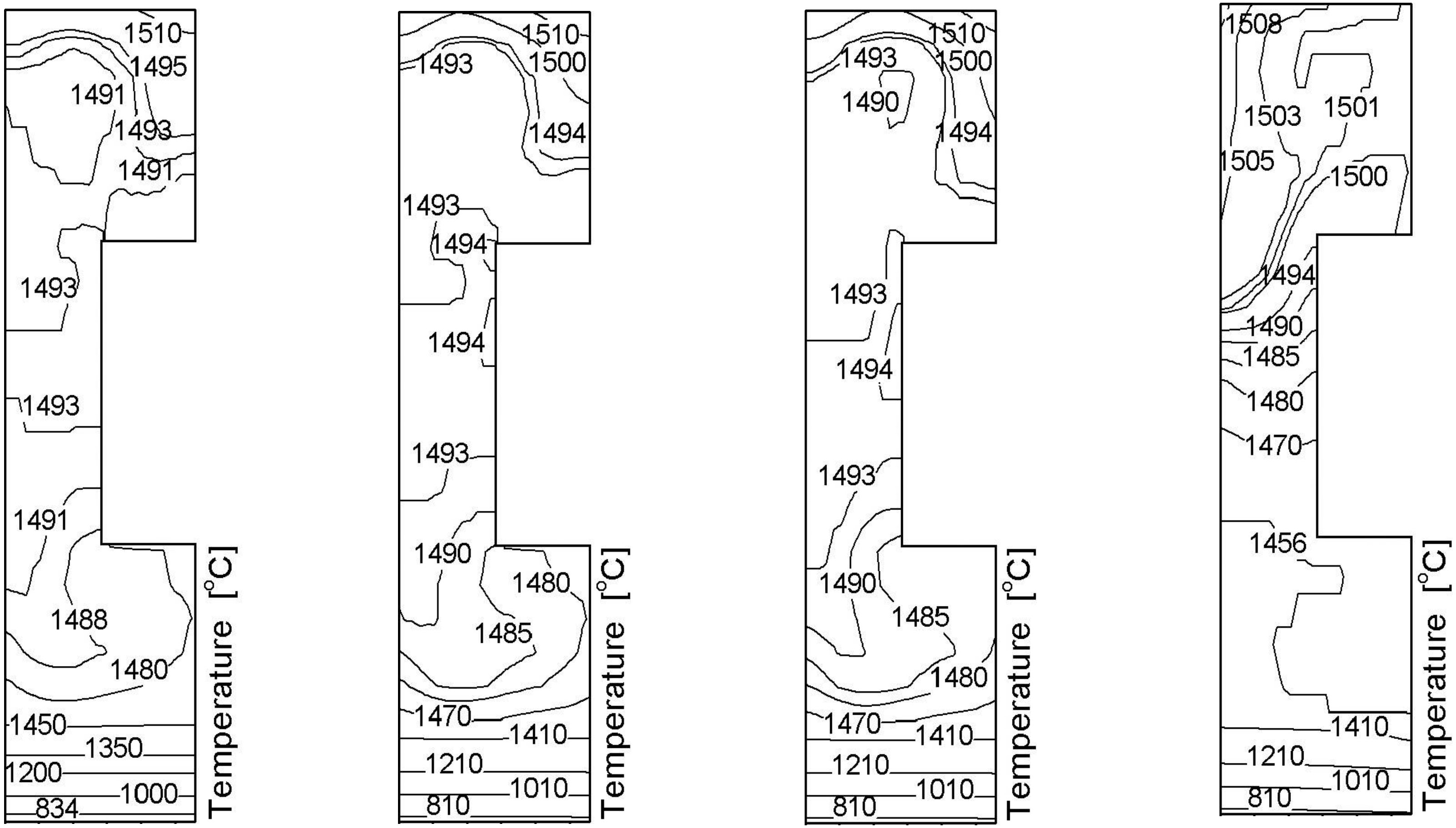

0At 1000At 2500At 10000At

Contours of Temperature at ~21.0 sec

Directional Solidification Transport Behaviors under Harmonic EM-fields of Different Current Loads. γ(TiAl)-55Al%at. , 20kHz

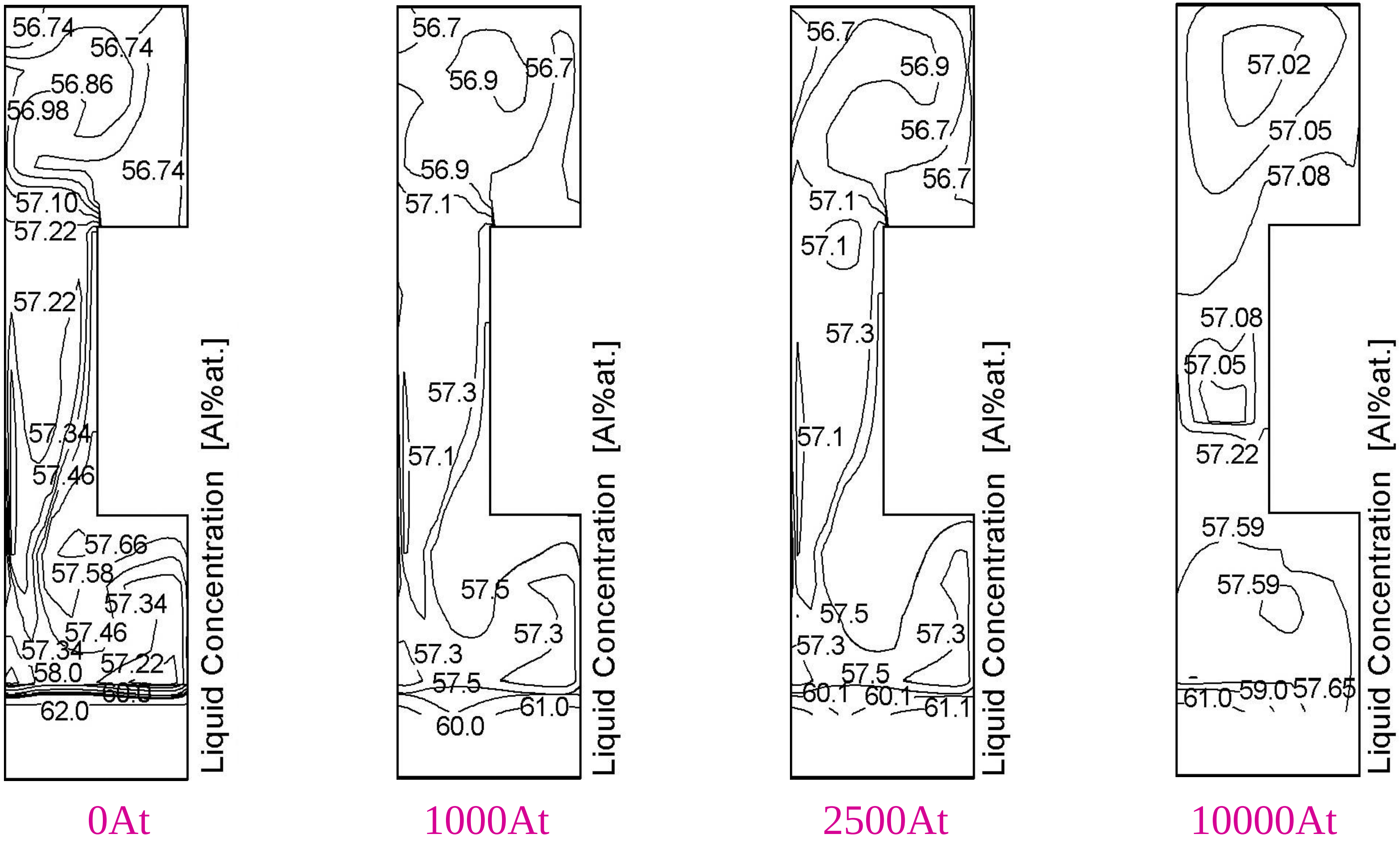

Contours of Liquid Concentration at ~21.0 sec

Animation: V&f_S Evolution in a Blade-like γ(TiAl)-55at.%Al Casting directionally Solidifying under Zero & a Harmonic EM-Field

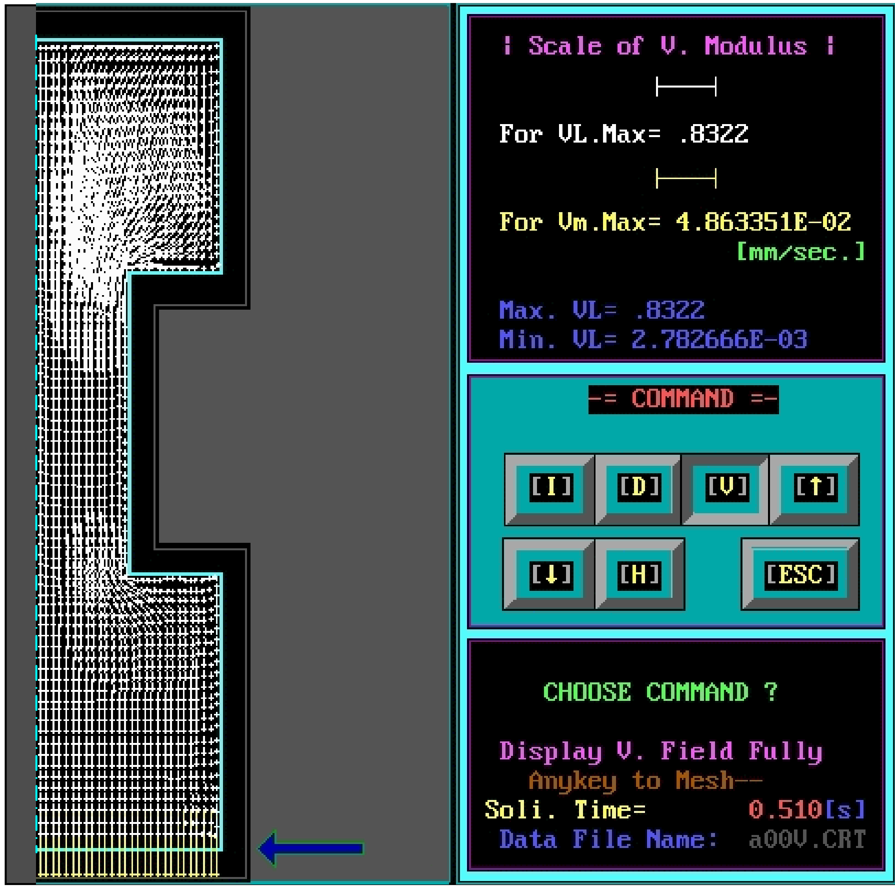

Only under Gravity

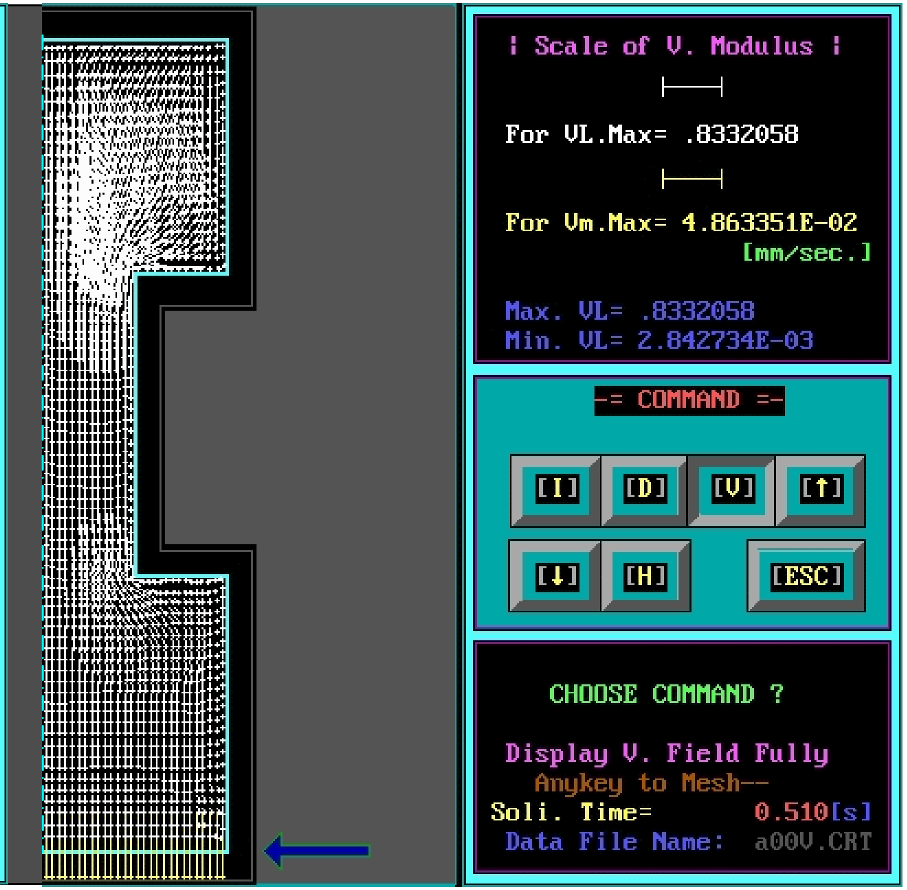

Under Gravity + Harnonic EM-Field (20kHz,500kAt)

Solidification Transport Processes of a Blade-like Al-4.5%Cu Casting under Transverse Static Magnetic Fields of different Load Strengths (in At)

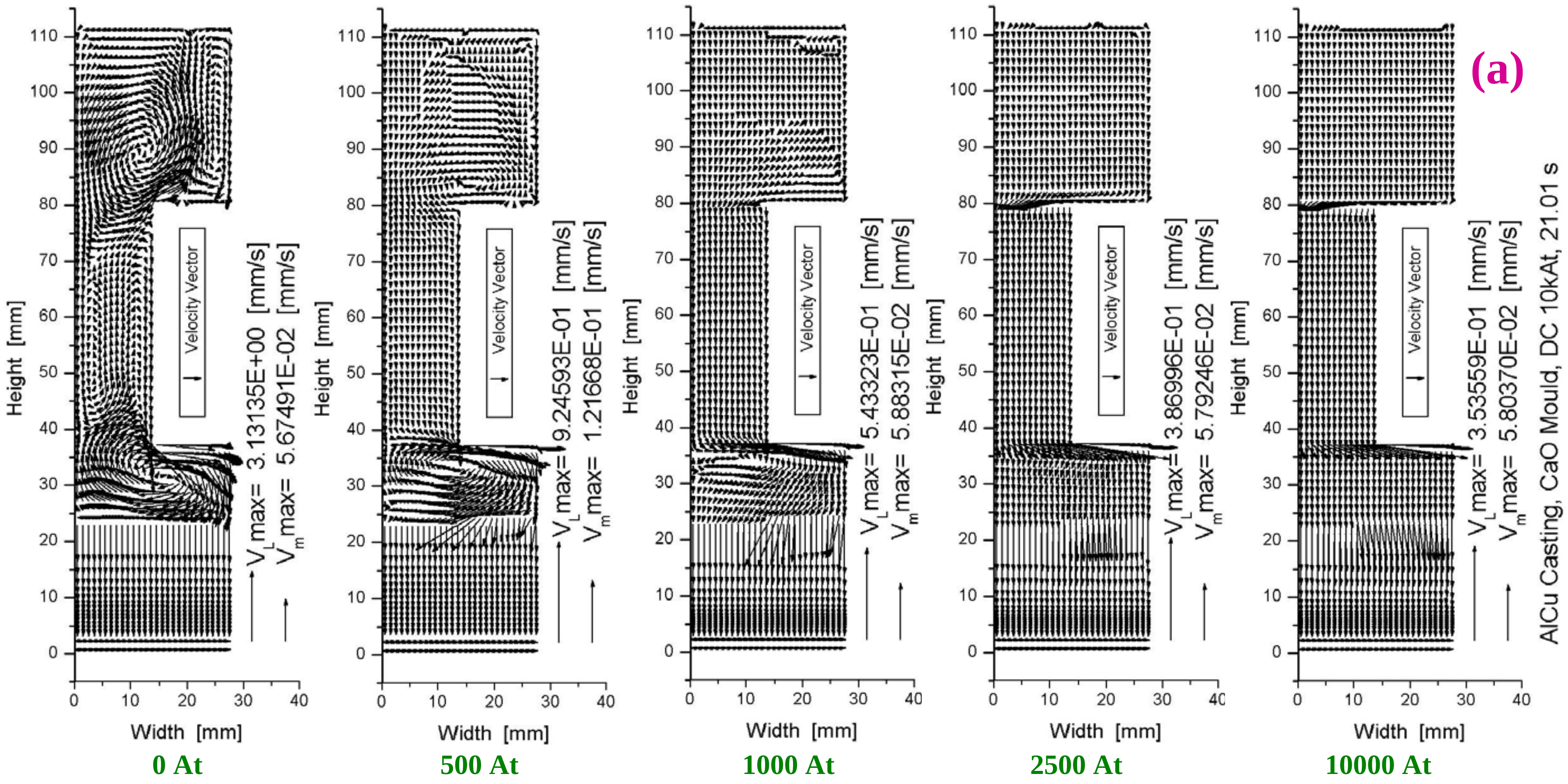

Comparisons of liquid flow and directional solidification behaviors of Al-4.5%Cu shaped casting under static magnetic fields inducted by different current-turns at t=21.0 sec: (a) Velocity vectors of liquid phases; (b) Contours of relative pressure in the liquid; (c) Contours of solid volume fraction; (d) Contours of temperature.

Solidification Transport Processes of a Blade-like Al-4.5%Cu Casting under Transverse Static Magnetic Fields of different Load Strengths (in At)

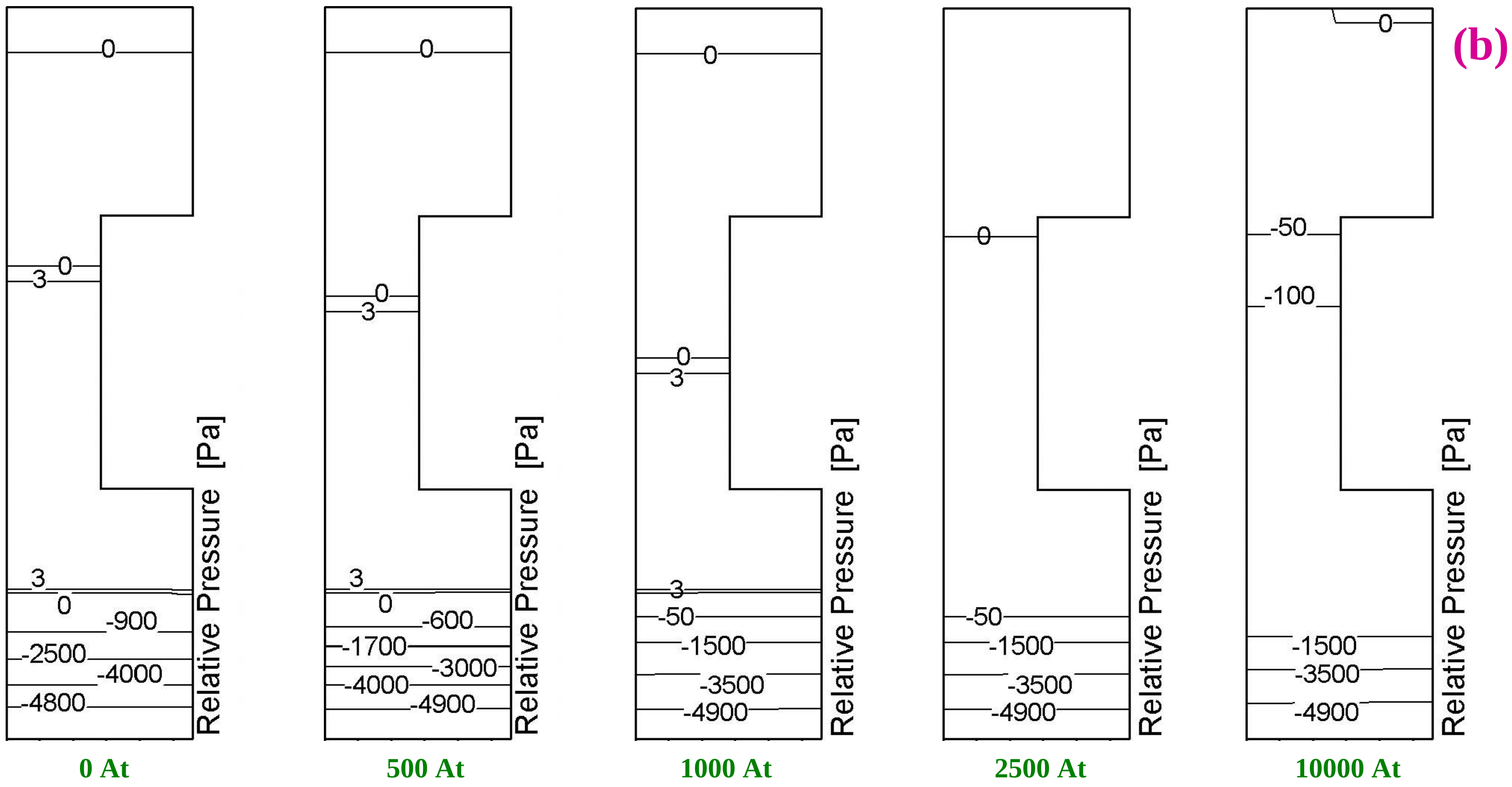

Comparisons of liquid flow and directional solidification behaviors of Al-4.5%Cu shaped casting under static magnetic fields inducted by different current-turns at t=21.0 sec: (a) Velocity vectors of liquid phases; (b) Contours of relative pressure in the liquid; (c) Contours of solid volume fraction; (d) Contours of temperature.

Solidification Transport Processes of a Blade-like Al-4.5%Cu Casting under Transverse Static Magnetic Fields of different Load Strengths (in At)

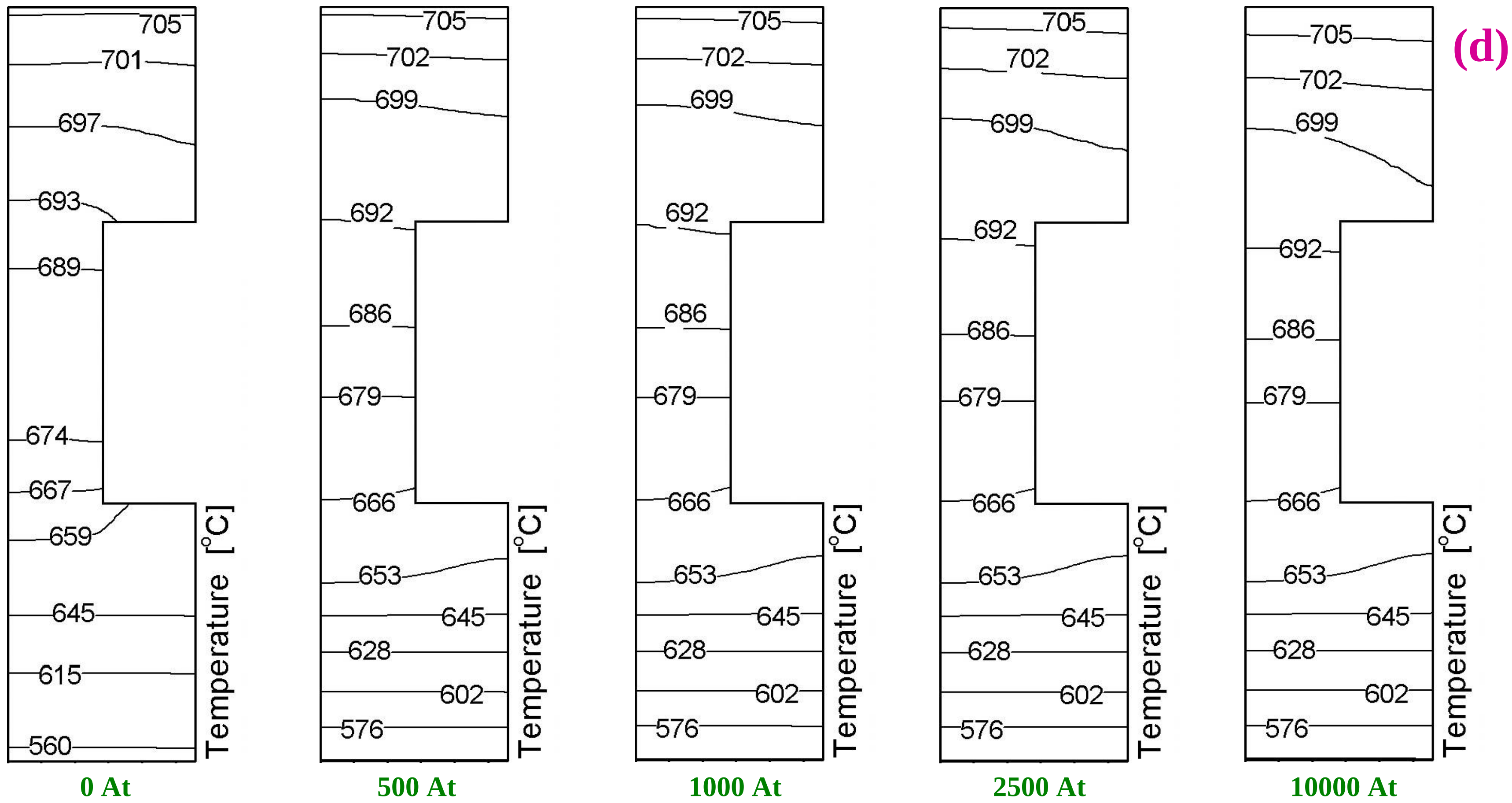

Comparisons of liquid flow and directional solidification behaviors of Al-4.5%Cu shaped casting under static magnetic fields inducted by different current-turns at t=21.0 sec: (a) Velocity vectors of liquid phases; (b) Contours of relative pressure in the liquid; (c) Contours of solid volume fraction; (d) Contours of temperature.

Solidification Transport Processes of a Blade-like In718-4.85%Nb Casting under Transverse Static Magnetic Fields of different Load Strengths (in At)

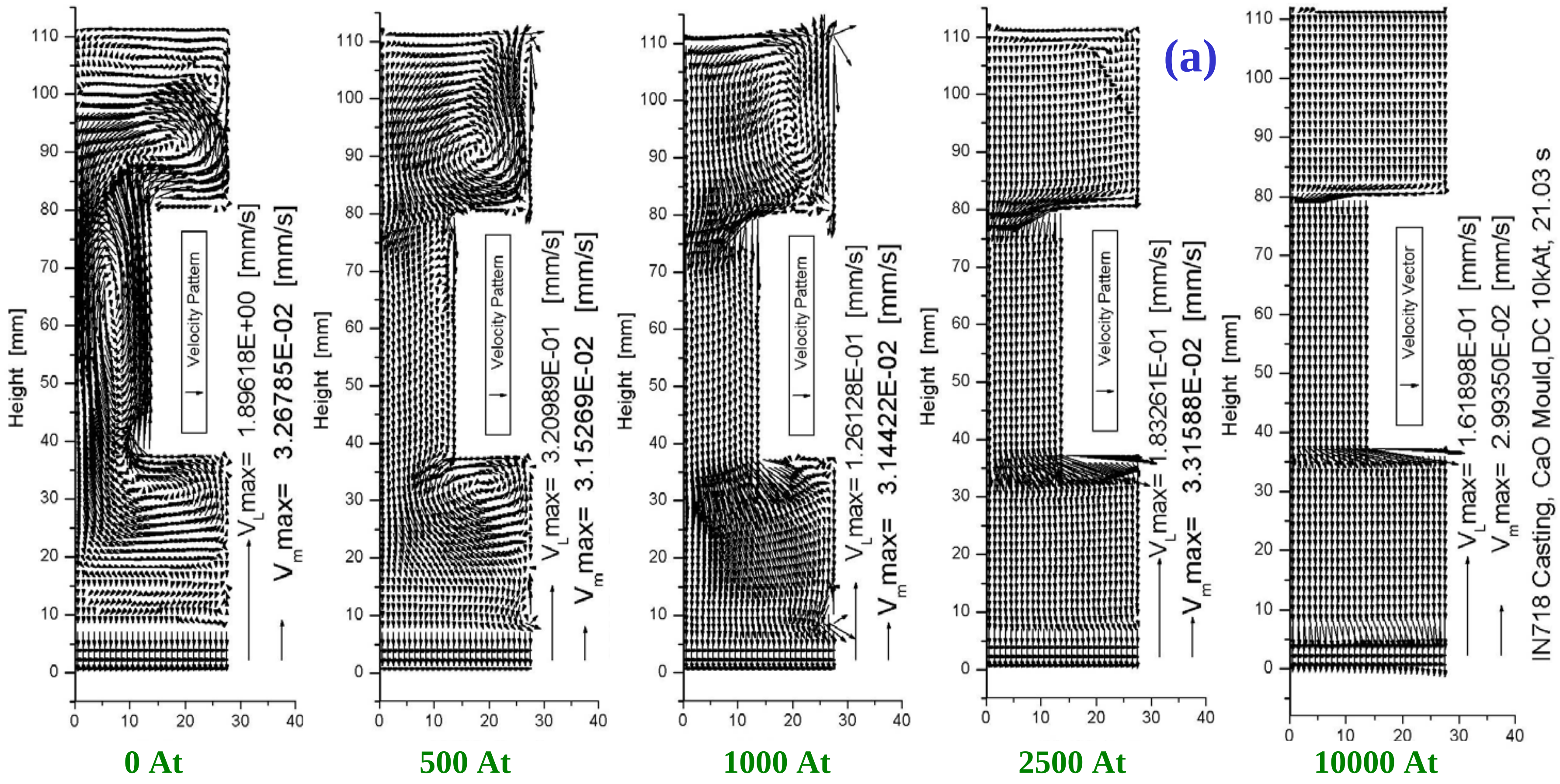

Influences of transverse static magnetic strengths on the liquid flow behaviors and temperature /concentration distributions in directionally solidified In718 shaped castings at t=21.0 sec.: (a) Velocity vectors of liquid phases; (b) Contours of temperature; (c) Contours of liquid concentration, Nb%wt..

Solidification Transport Processes of a Blade-like In718-4.85%Nb Casting under Transverse Static Magnetic Fields of different Load Strengths (in At)

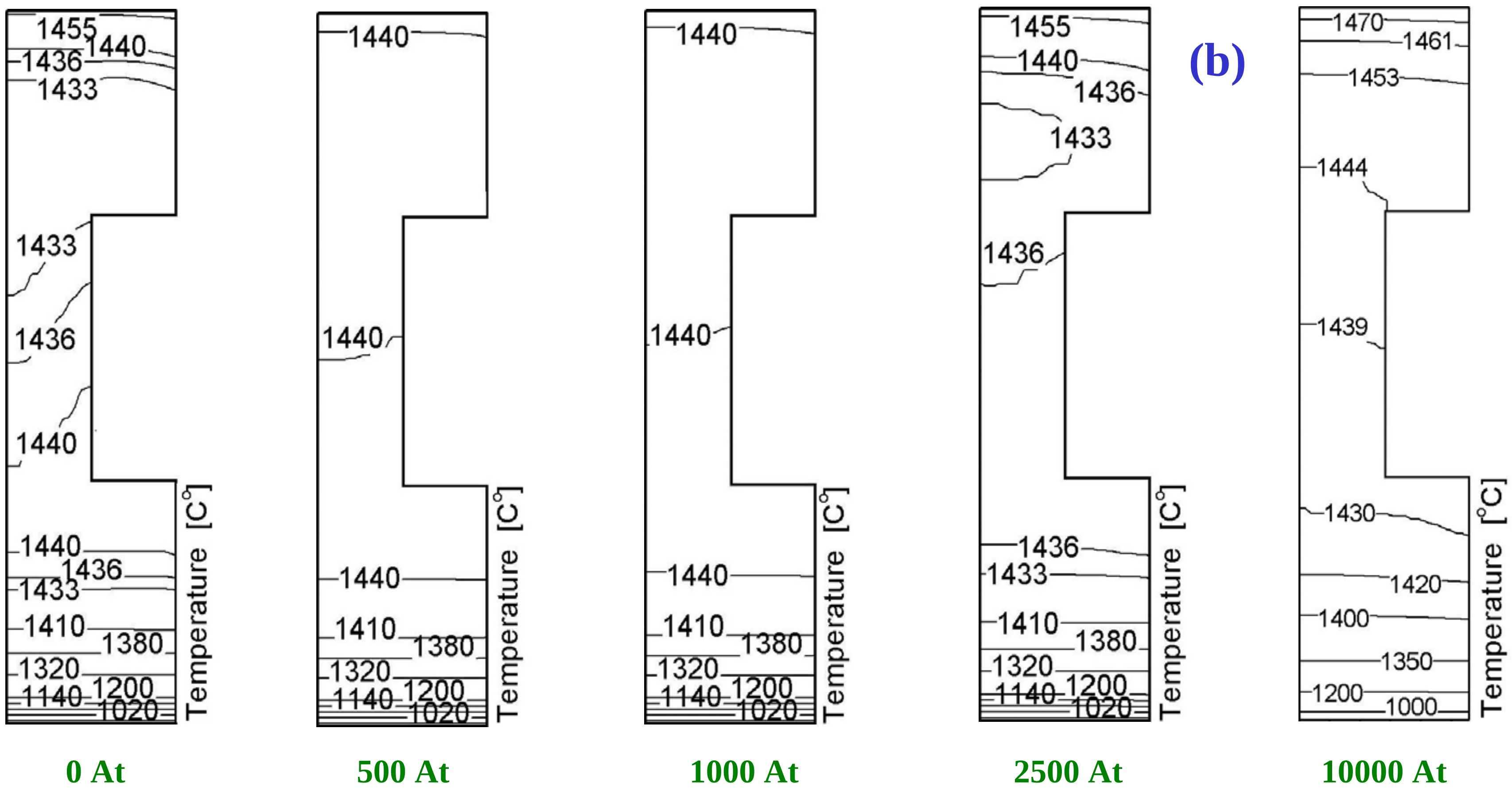

Influences of transverse static magnetic strengths on the liquid flow behaviors and temperature /concentration distributions in directionally solidified In718 shaped castings at t=21.0 sec.: (a) Velocity vectors of liquid phases; (b) Contours of temperature; (c) Contours of liquid concentration, Nb%wt..

Solidification Transport Processes of a Blade-like In718-4.85%Nb Casting under Transverse Static Magnetic Fields of different Load Strengths (in At)

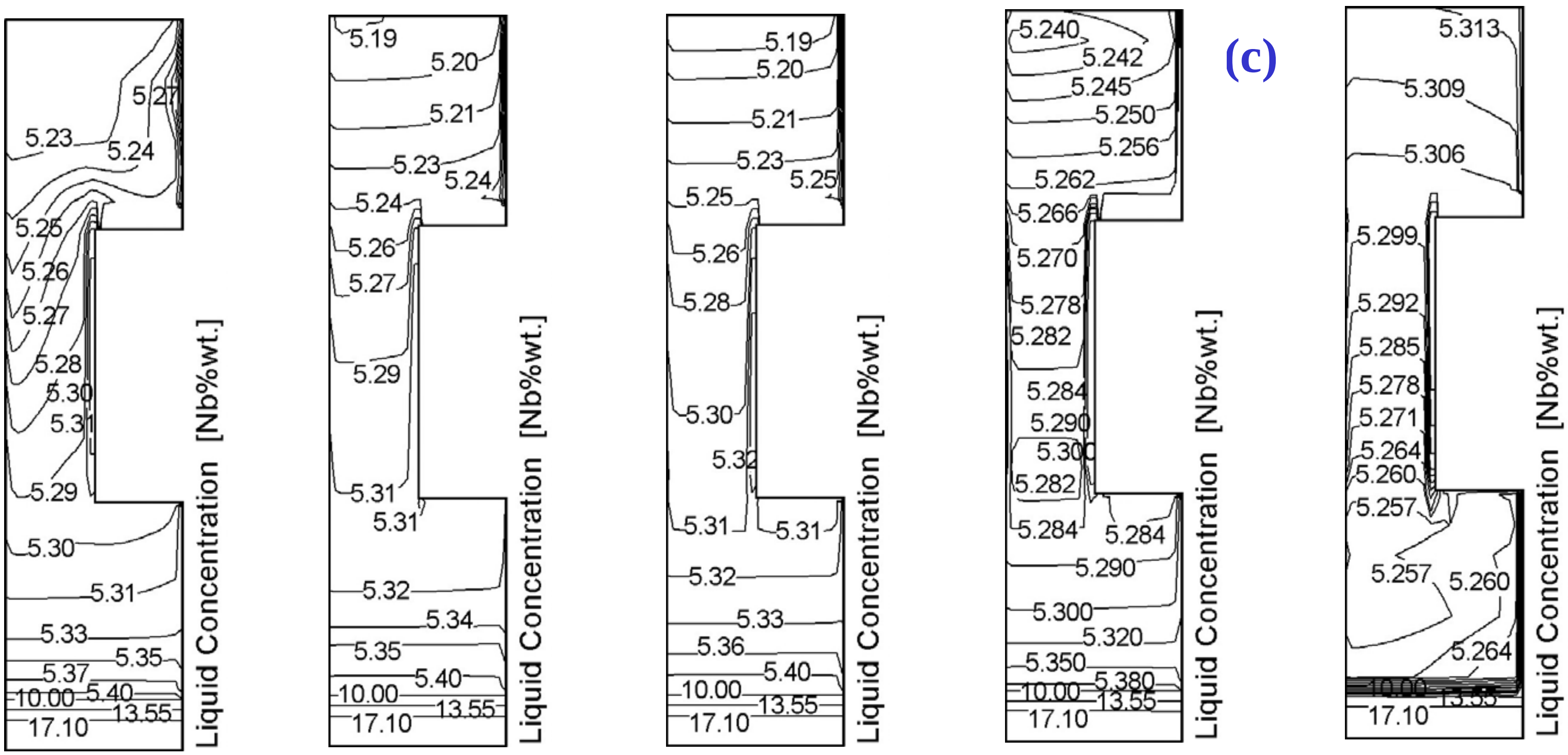

0 At **500 At** **1000 At** **2500 At** **10000 At**

Influences of transverse static magnetic strengths on the liquid flow behaviors and temperature /concentration distributions in directionally solidified In718 shaped castings at t=21.0 sec.: (a) Velocity vectors of liquid phases; (b) Contours of temperature; (c) Contours of liquid concentration, Nb%wt..

Application on the Way to:

Directional Solidification of Cold Crucible Titanum Alloy Strip Ingot

Directional Solidification Apparatus of Cold Crucible Ti Alloy Strip Ingot Currently Used in the Authors' Group

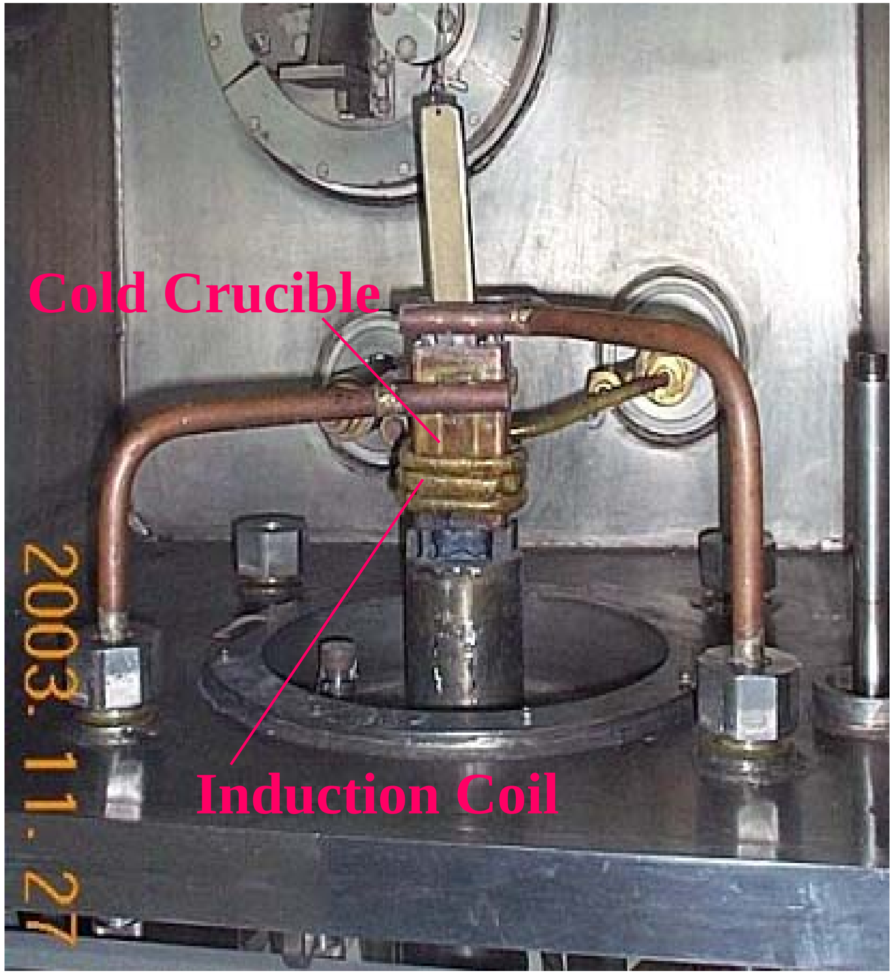

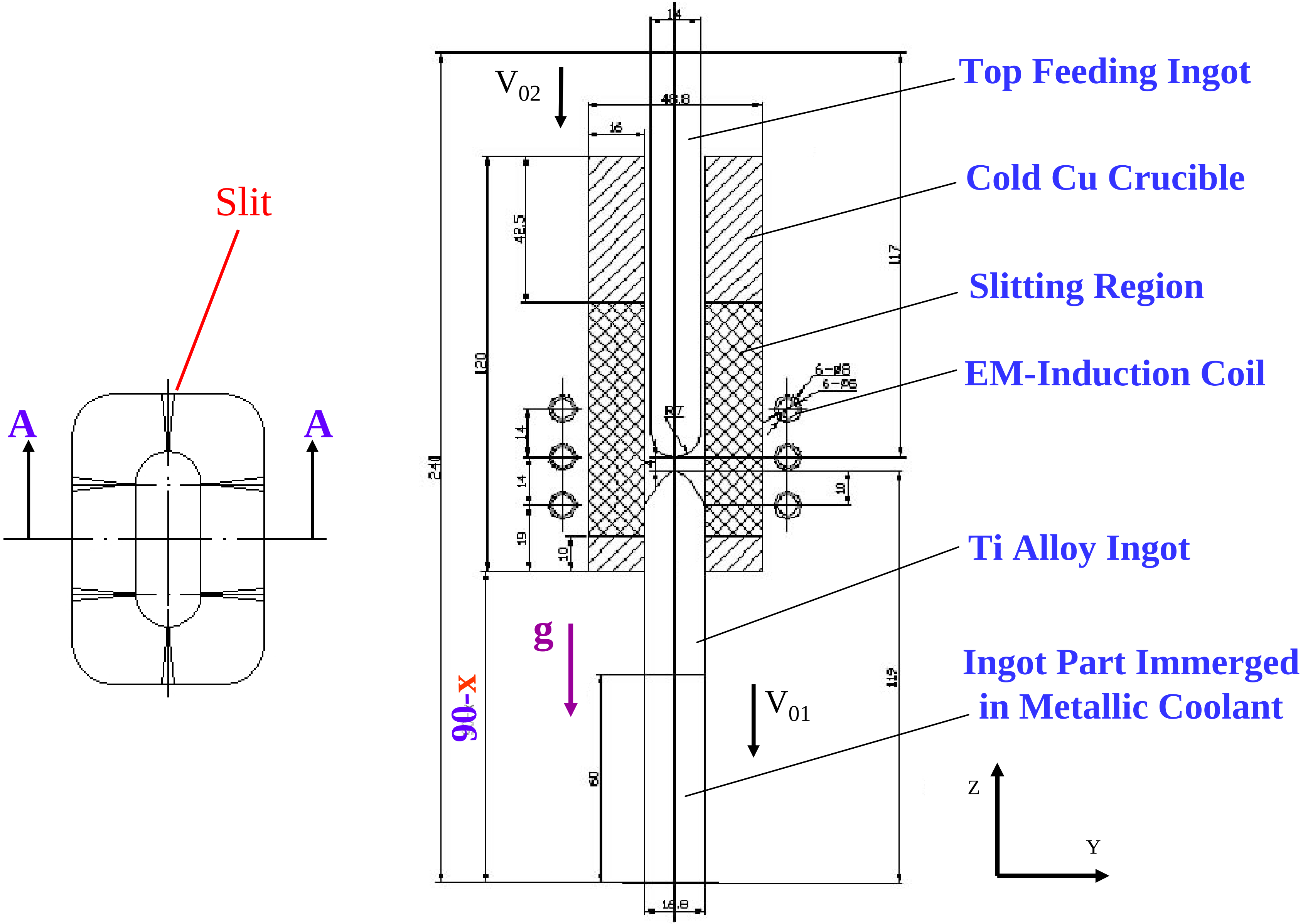

A Simplified 2-D Configuration for Directional Solidification of Cold Crucible Ti Alloy Strip Ingot

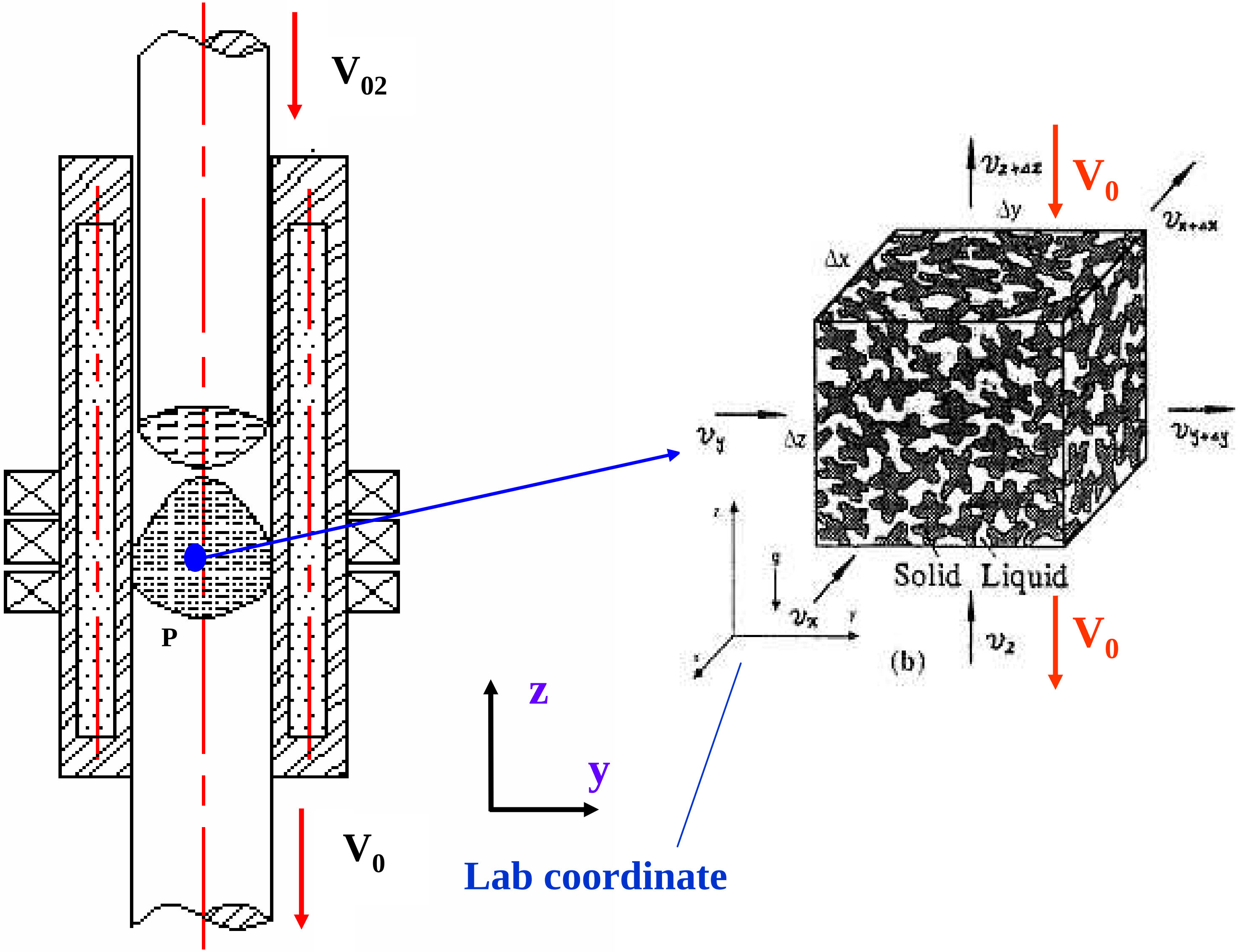

Schematic EM-Directional Solidification Configuration for Continuum Model Revision

Revised Continuum Model for EM-STP

Solidification heat energy transfer

$$\partial[(\rho c_p)_m]/\partial t + \nabla(f_L\rho_L c_{pL} VT) + V_0\partial[(f_L\rho_L c_{pL} T) + (f_S\rho_S c_{pS} T)]/\partial z$$
$$= \nabla[k_m \nabla T] + \rho_S h(\partial f_S/\partial t) + q_J$$

Solidification solute mass transfer

$$\partial[(\rho C)_m]/\partial t + \nabla(f_L\rho_L C_L V) + V_0\partial[(f_L\rho_L C_L) + (f_S\rho_S C_S)]/\partial z$$
$$= \nabla[\rho_L D_L \nabla(f_L C_L) + \rho_S D_S \nabla(f_S\rho_S C_S)]$$

Solidification mass conservation

$$\partial\rho/\partial t + \nabla(f_L\rho_L V) + V_0\partial\rho/\partial z = 0$$

Momentum transfer for bulk/interdendritic liquid flow

$$\partial(f_L\rho_L V)/\partial t + \nabla[(f_L\rho_L V)V] + V_0 \nabla(f_L\rho_L V) + V_0\partial(f_L\rho_L V)/\partial z$$
$$= \nabla[\mu \nabla(f_L V) - \nabla(f_L P) + f_L\rho_L g - (\mu f_L^2/K)V + f_L\rho_L g + F_L$$

Schematic FEM and FDM Meshing for the Top and Bottom Hump Regions

F
E
M

M
E
S
H
I
N
G

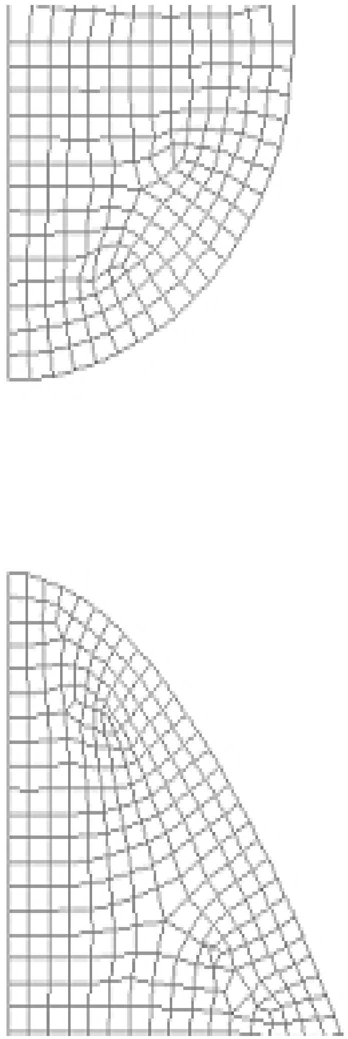

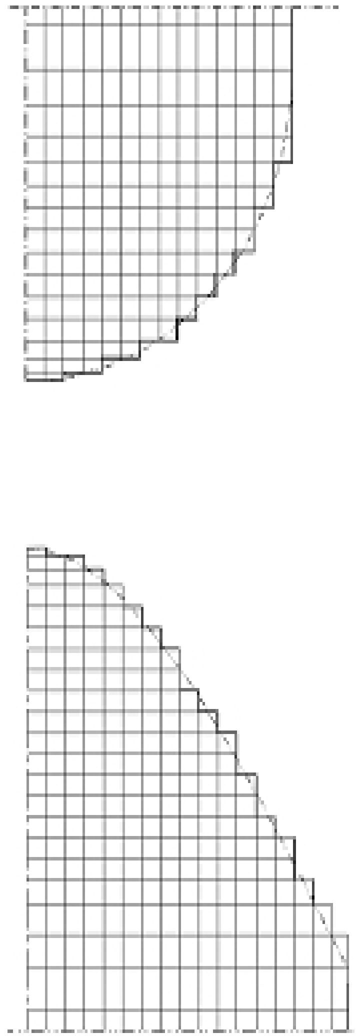

F
D
M

M
E
S
H
I
N
G

Magnetic Flux Density Vectors Output from Ansys 6.1 FEM-Analysis

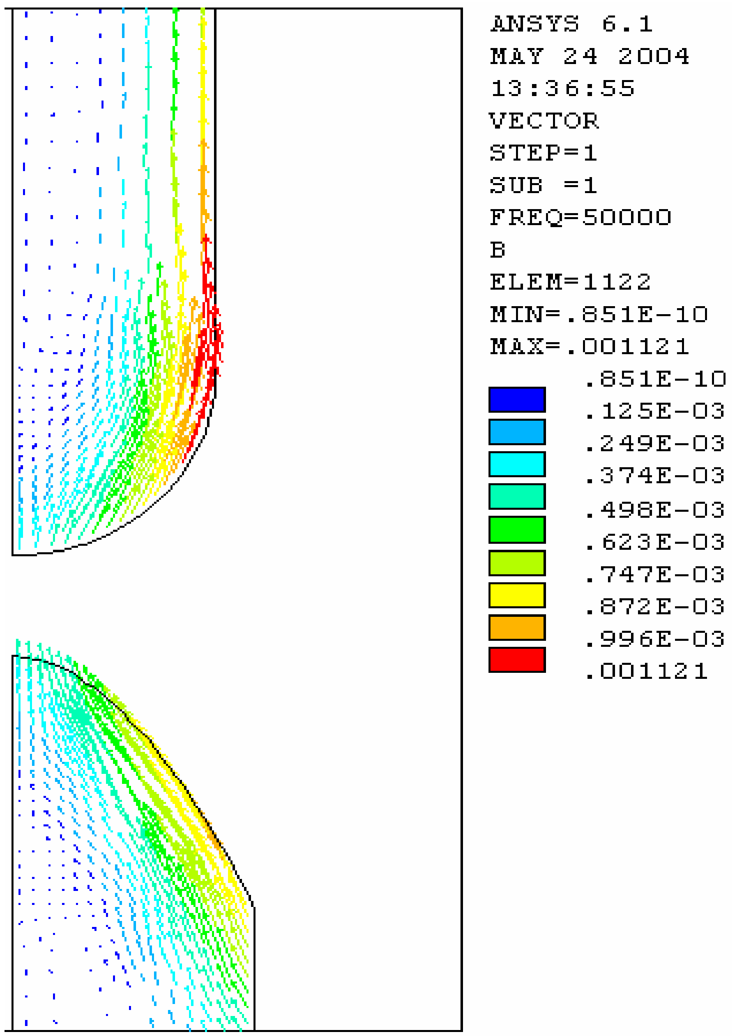

$\rho_E = 2 \times 10^{-5}\ \Omega m$

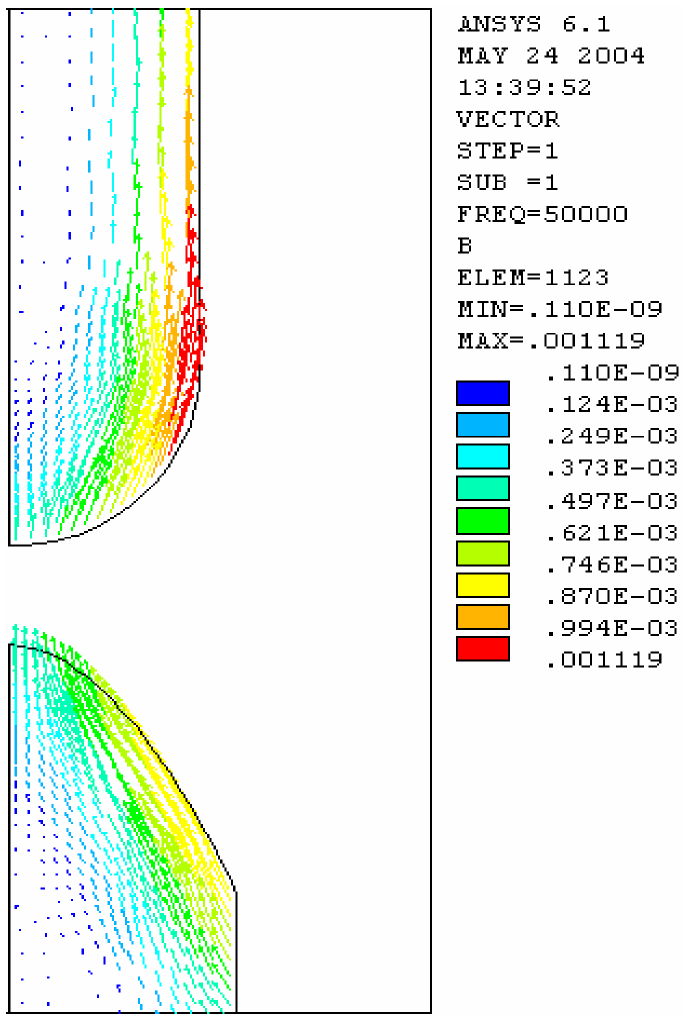

$\rho_E = 2.5 \times 10^{-5}\ \Omega m$

EM-FEM q_J Results→FDM Format Conversion

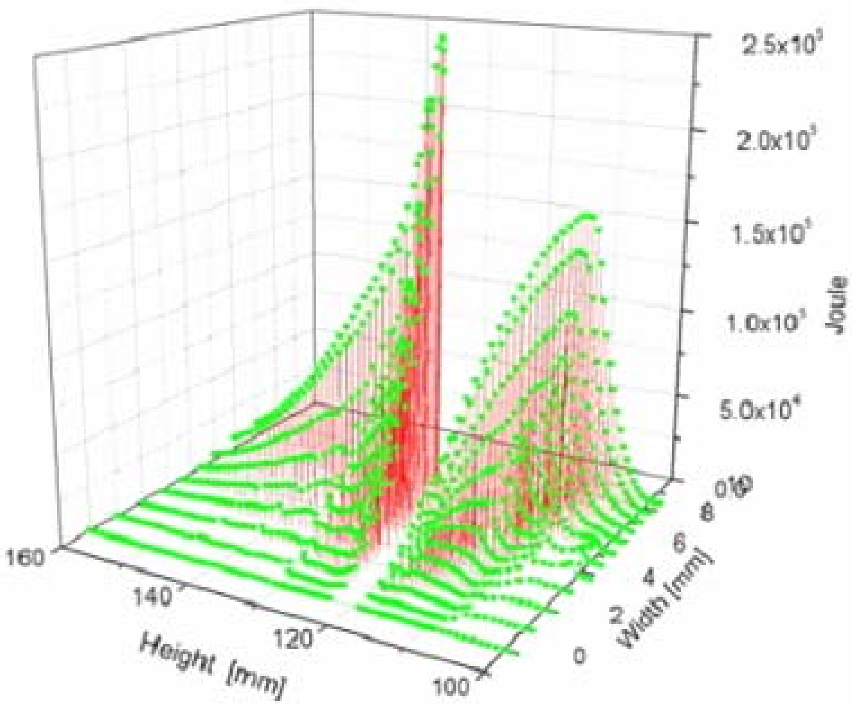

Ansys FEM-Results

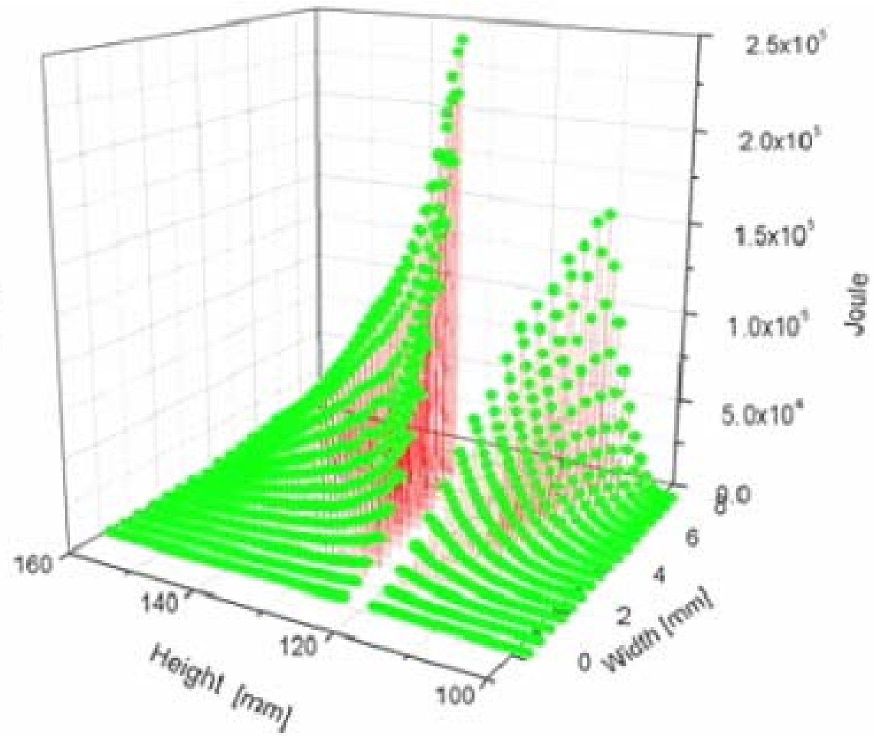

Converted FDM Results

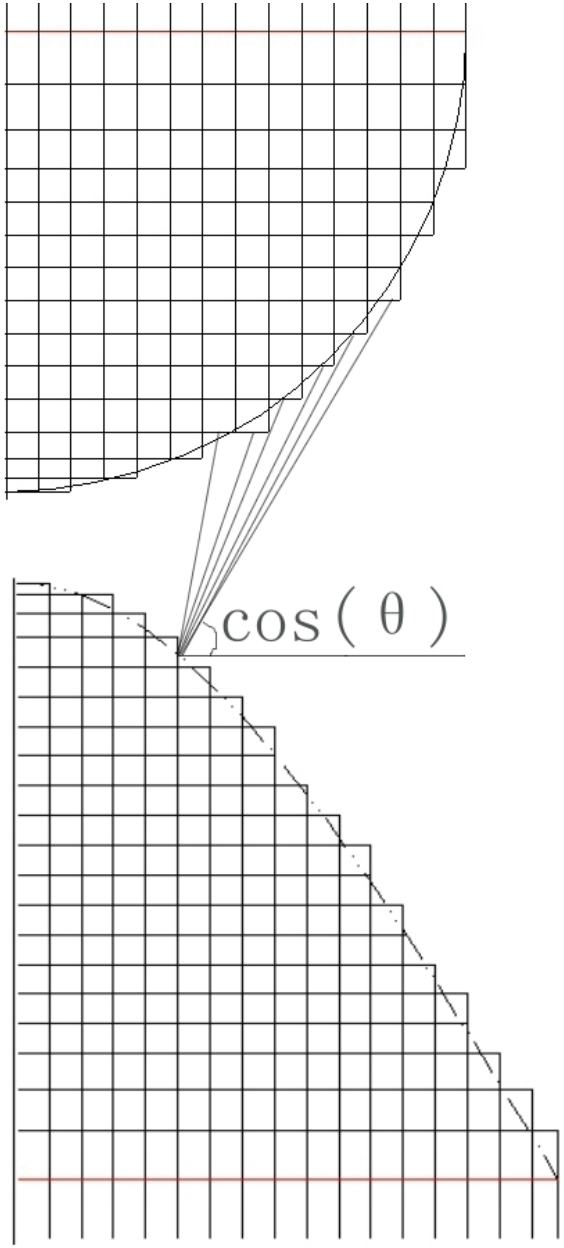

Schematic Radiation Heat Transfer between the Top and Bottom Humps

$$T = (\alpha \sum_{JI+1}^{JI2} T_{J,K+1/2} + T_M)/[\alpha(JI2-1-JI)+1]$$

α is an approximate average of the sum of view factor cosθ (0<α<1)

EM-Inducted Heating Processes in Top and Bottom Ingots (at x=12mm)

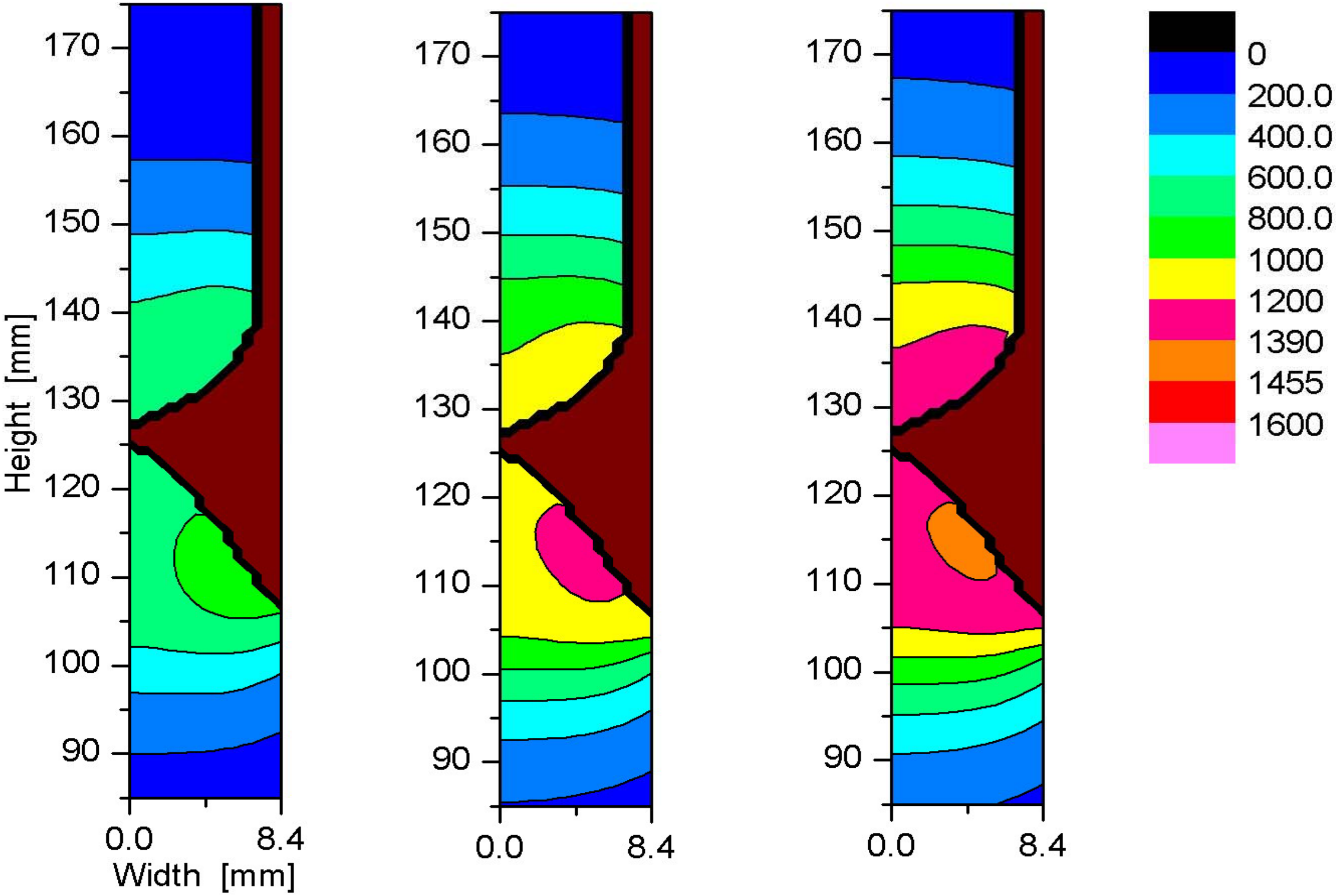

a) 10 sec. **b) 20 sec.** **c) 30 sec.**

EM-Inducted Heating Processes in Top and Bottom Ingots (at x=12mm)

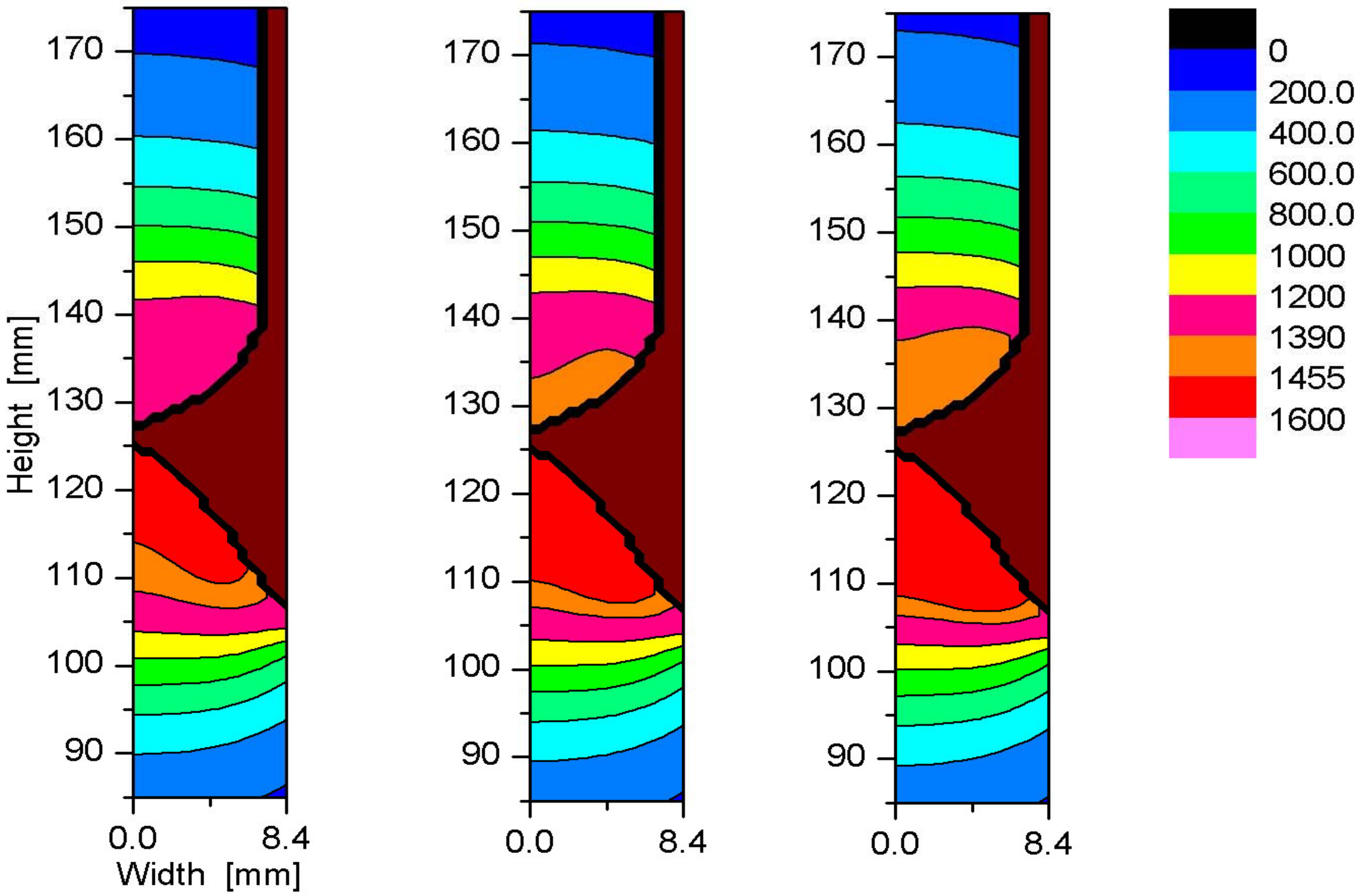

d) 40 sec. **e) 50 sec.** **f) 60 sec.**

EM-Inducted Heating Processes in Top and Bottom Ingots (at x=12mm)

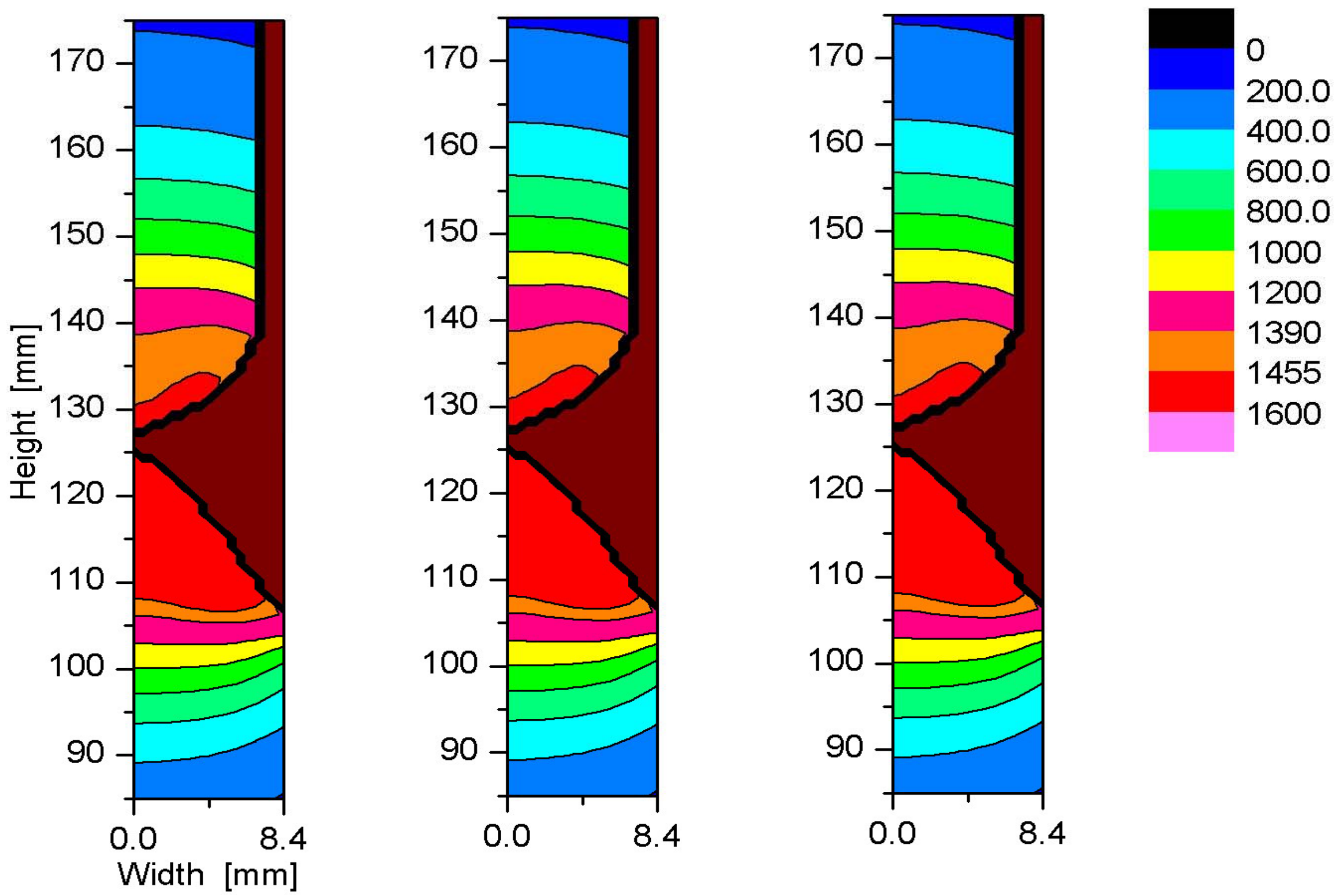

g) 100 sec. h) 130 sec. i) 170 sec.

Summary

- The proposed modeling methods appear practical and efficient in numerical computation (The each above demonstrated sample usually takes 2-5 hours on a PC with a 1.6GHz-CPU)
- The computational results show that the solidification-shrinkage-driven interdendritic liquid flow in mushy zone, though usually smaller than the convection in bulk liquid region by order(s), can not be easily suppressed by a static magnetic field applied. (The inner force caused by solidification-shrinkage might be much stronger than Lorentz force)

Thank you

Table I Initial and technological parameters for the present example simulations with 3 different kinds of Alloys

Alloys	IN718 base-4.85wt.%Nb	γ(TiAl)-55at.%Al	Al-4.5wt.%Cu
Pouring temperature, T_P	1450 °C	1500 °C	700 °C
Initial mold temperature, T_M	1500 °C	1550 °C	700 °C
Heating zone temperature, T_h	1600 °C	1600 °C	950 °C
Cooling zone temperature, T_C	45 °C	45 °C	25 °C
Bottom cooler temperature, T_{BC}	45 °C	45 °C	25 °C
Withdrawal velocity, V_0	0.15 mm/sec	0.15 mm/sec	0.15 mm/sec

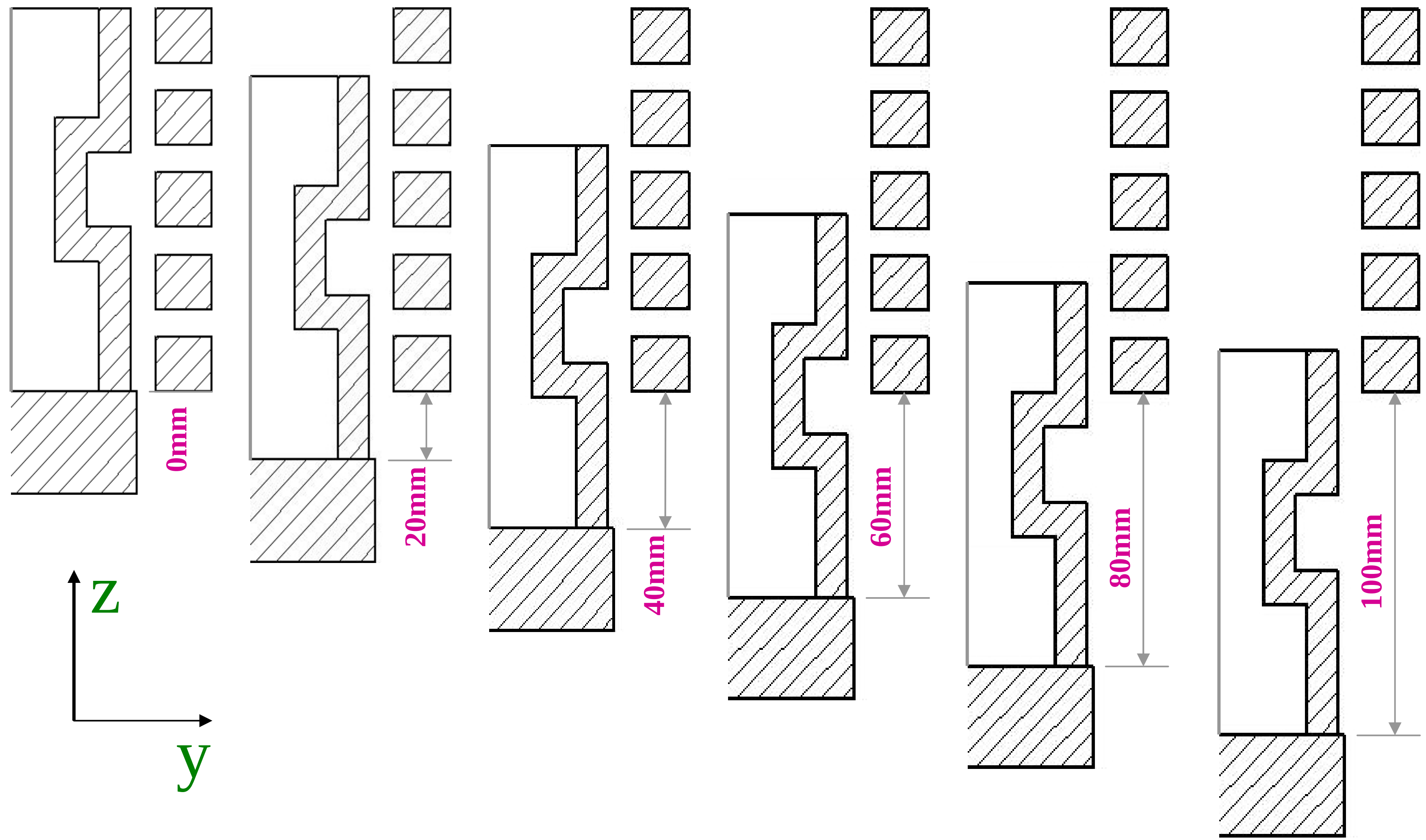

Configurations of Directionally Solidifying Blade-like Alloy Casting under a Harmonic EM-Field at Different Withdrawal Positions —At Each Position, an Ansys EM-FEM Analysis Made for EM-Field Interpolations for the Continuous EM-Solidification Process

Free Surface Tension:

Determining the free surface morphology of alloy melt corporately with gravity/ Lorentz force and the dynamic pressure resulted from the melt flow.

(in a continuously changing state)

The Force Balance on a Free Surface of Alloy Melt:

表面张力 + 熔体的静、动压力 + 电磁力(Lorentz力) = 0

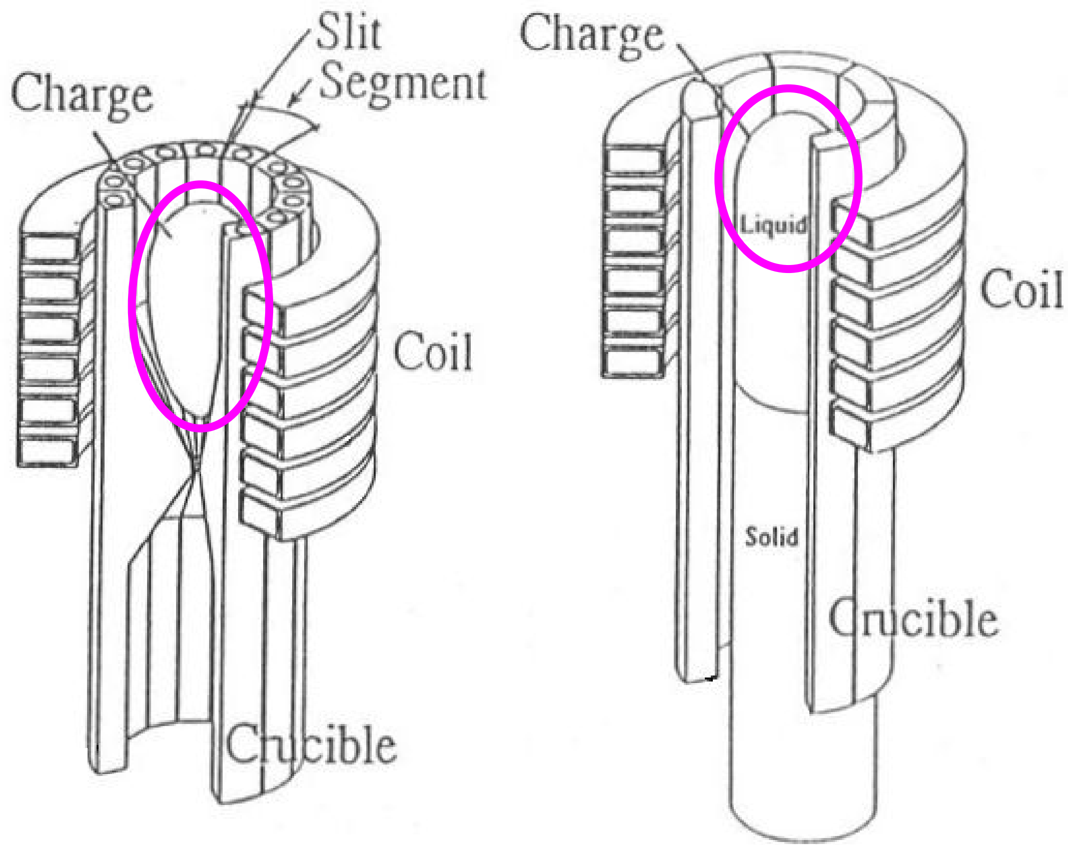

Two types of Cold Crucible Processes

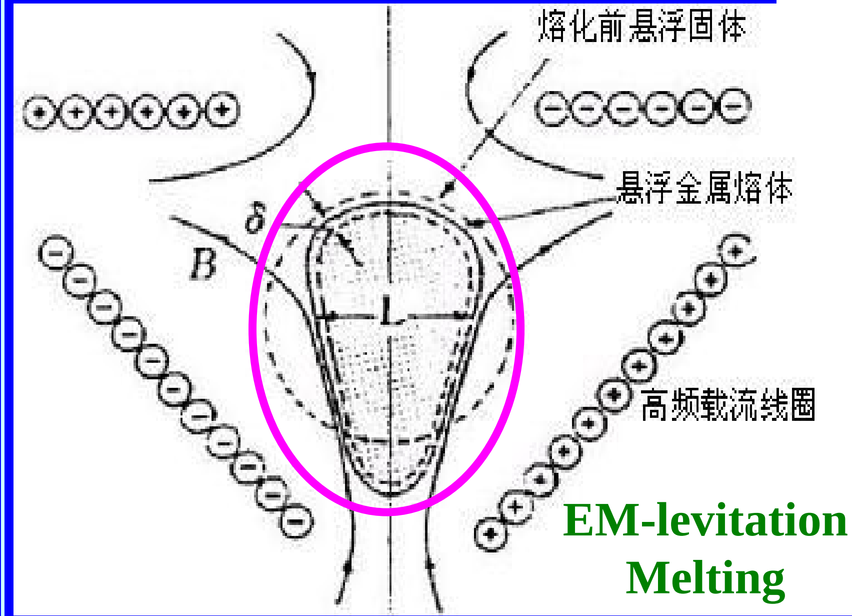

EM-levitation Melting

Fully numerical description for a 3-D free surface morphology of alloy melt in a dynamically changing state is a stiff task for the modelers in materials metallurgy and solidification fields.

"Liquid Metal Flow with Heat Transfer in a Cold Crucible Confined by a Free Surface and a Solidification Front",

by T. TANAKA *et al*, *ISIJ International*, 1991, v.31, pp.1416-1423.

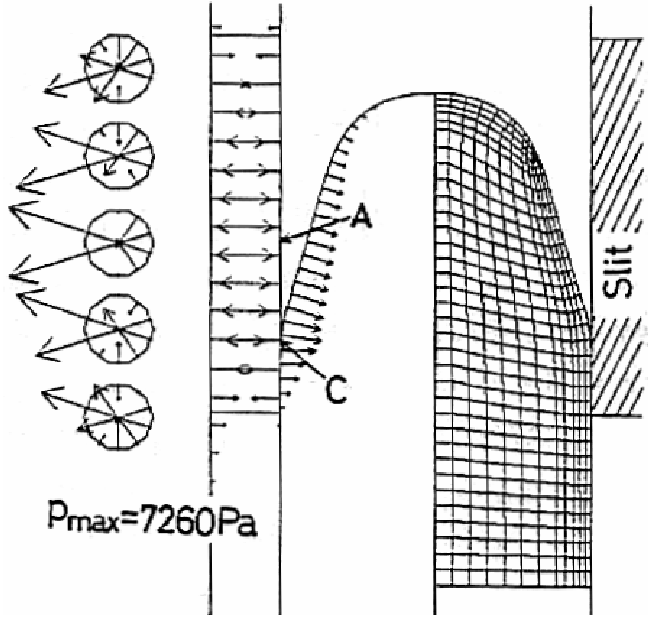

Configuration and mesh used for calculating the fields of velocity and temperature

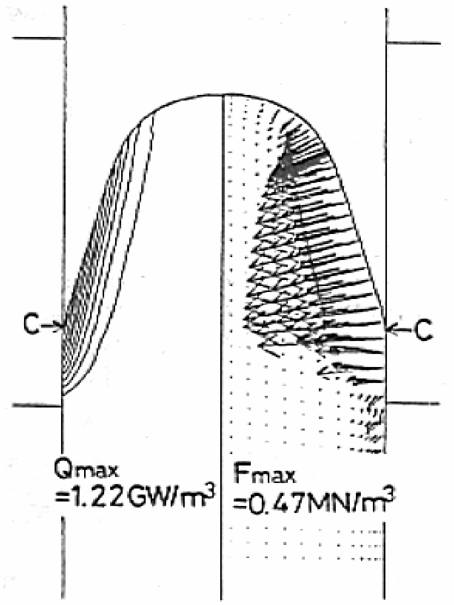

Calculated contours of Joule heat and magnetic body force

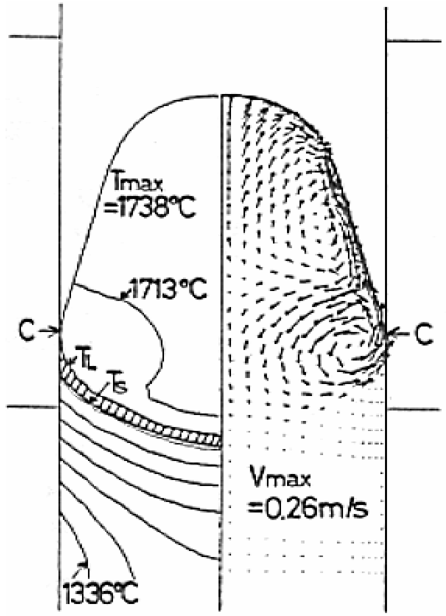

Calculated fields of temperature and velocity in a Melt